Available online at www.sciencedirect.com
ScienceDirect
Journal of Colloid and Interface Science 312 (2007) 363–380
JOURNAL OF Colloid and Interface Science
www.elsevier.com/locate/jcis

Emulsification in turbulent flow
1. Mean and maximum drop diameters in inertial and viscous regimes

Nina Vankova [a], Slavka Tcholakova [a], Nikolai D. Denkov [a,*], Ivan B. Ivanov [a], Vassil D. Vulchev [b], Thomas Danner [c]

[a] *Laboratory of Chemical Physics & Engineering, Faculty of Chemistry, Sofia University, 1 James Bourchier Ave., 1164 Sofia, Bulgaria*
[b] *Faculty of Physics, Sofia University, 1164 Sofia, Bulgaria*
[c] *BASF Aktiengesellschaft, GCT/P, L549, Ludwigshafen, Germany*

Received 20 October 2006; accepted 24 March 2007

Available online 30 March 2007

Abstract

Systematic experimental study of the effects of several factors on the mean and maximum drop sizes during emulsification in turbulent flow is performed. These factors include: (1) rate of energy dissipation, ε; (2) interfacial tension, σ; (3) viscosity of the oil phase, η_D; (4) viscosity of the aqueous phase, η_C; and (5) oil volume fraction, Φ. The emulsions are prepared by using the so-called "narrow-gap homogenizer" working in turbulent regime of emulsification. The experiments are performed at high surfactant concentration to avoid the effect of drop–drop coalescence. For emulsions prepared in the *inertial* turbulent regime, the mean and the maximum drop sizes increase with the increase of η_D and σ, and with the decrease of ε. In contrast, Φ and η_C affect only slightly the mean and the maximum drop sizes in this regime of emulsification. These results are described very well by a theoretical expression proposed by Davies [Chem. Eng. Sci. 40 (1985) 839], which accounts for the effects of the drop capillary pressure and the viscous dissipation inside the breaking drops. The polydispersity of the emulsions prepared in the inertial regime of emulsification does not depend significantly on σ and ε. However, the emulsion polydispersity increases significantly with the increase of oil viscosity, η_D. The experiments showed also that the inertial turbulent regime is inappropriate for emulsification of oils with viscosity above ca. 500 mPa s, if drops of micrometer size are to be obtained. The transition from inertial to viscous turbulent regime of emulsification was accomplished by a moderate increase of the viscosity of the aqueous phase (above 5 mPa s in the studied systems) and/or by increase of the oil volume fraction, $\Phi > 0.6$. Remarkably, emulsions with drops of micrometer size are easily formed in the *viscous* turbulent regime of emulsification, even for oils with viscosity as high as 10,000 mPa s. In this regime, the mean drop size rapidly decreases with the increase of η_C and Φ (along with the effects of ε, σ, and η_D, which are qualitatively similar in the inertial and viscous regimes of emulsification). The experimental results are theoretically described and discussed by using expressions from the literature and their modifications (proposed in the current study).

Keywords: Emulsification in turbulent flow; Drop breakup; Drop-size distribution; Emulsification in viscous regime; Kolmogorov theory of emulsification

1. Introduction

The emulsification process can be considered as consisting of two opposite "elementary reactions": drop breakup leading to formation of several smaller drops from a larger one, and drop–drop coalescence leading to formation of a larger drop from two smaller drops. In the general case, the evolution of the drop-size distribution during emulsification is governed by the competition of these two opposite processes [1–6]. At high surfactant concentrations, the contribution of the drop–drop coalescence is negligible and the process of drop breakup determines the evolution of the drop-size distribution in the formed emulsions. After a sufficiently long emulsification time, a "steady-state" is reached, which is characterized by a relatively slow change of the drop-size distribution in the formed emulsions. In the current study, we consider the mean and the maximum drop sizes (see below for precise definitions), obtained as a result of the drop-breakup process in turbulent flow, in the steady-state stage of the emulsification process. The com-

* Corresponding author. Fax: +359 2 962 5643.
E-mail address: nd@lcpe.uni-sofia.bg (N.D. Denkov).

0021-9797/$ – see front matter
doi:10.1016/j.jcis.2007.03.059

plementary study of the kinetics of drop-breakup in the same systems, which requires more elaborate analysis of the drop-breakup process, is presented in two subsequent papers [7,8]. For discussion of the kinetic aspects of reaching the steady-state period in the actual emulsification experiments, see Refs. [9–11] and Section 4 in Ref. [7].

The classical studies of the emulsification process in turbulent flow, performed by Kolmogorov [12] and Hinze [13], showed that two different regimes of emulsification should be distinguished, which are termed "turbulent inertial" and "turbulent viscous" regimes, respectively (see Fig. 1). In the turbulent inertial regime, the drops are larger in diameter than the smallest turbulent eddies in the continuous phase, whereas in the turbulent viscous regime the drop diameter is smaller than the size of the smallest eddies. In the turbulent inertial regime, the maximum diameter of the stable drops (those able to resist the disruptive forces of the flow) is determined by the balance between the fluctuations in the hydrodynamic pressure of the continuous phase (which act on drop surface and induce drop deformation), and the drop capillary pressure, which opposes the drop deformation [12,13]. In contrast, in the turbulent viscous regime, the maximum diameter of the stable drops is determined by the balance between the viscous stress acting from the continuous phase on the drop surface and the drop capillary pressure. The transition between these two regimes of emulsification depends on the size of the smallest eddies in the turbulent flow, λ_0 (determined mainly by the rate of energy dissipation, ε, and the viscosity of the aqueous phase, η_C) and on the maximum drop size of the formed emulsion—see Section 2 for the respective equations.

Theoretical expressions relating the maximum diameter of the stable drops with the rate of energy dissipation, ε (which characterizes the intensity of the turbulent flow in Kolmogorov's theory), and with the interfacial tension of the drops, σ, were derived for these two regimes of emulsification, see Eqs. (4)–(6) below [12,13]. The expression for the inertial turbulent regime was verified experimentally by several investigators [14,15] for oil drops with viscosity close to that of the continuous aqueous phase, $\eta_D/\eta_C \sim 1$, and at relatively low oil volume fraction, $\Phi \leqslant 0.01$.

The theory of emulsification of more viscous drops, $\eta_D/\eta_C \gg 1$, in the inertial regime, was further developed by Davies [16], Lagisetty et al. [17] and Calabrese et al. [18–21]—see Section 2 below. Large set of experimental results for the effects of drop viscosity and interfacial tension on the maximum drop diameter was presented in the papers by Calabrese et al. [18–21], and a good description by the theoretical expressions was observed.

The studies on the oil emulsification in turbulent viscous regime are scarce [22–24]. In this regime, the drops should be smaller than the size of the turbulent eddies, which means that higher rate of energy dissipation is required to achieve this regime, at fixed viscosity of the aqueous phase and drop size [22–24]. On the other hand, different dependences of the maximum drop size on the various governing parameters were derived for these two regimes of emulsification (Eqs. (4) and (6) below), which predict that smaller droplets could be formed

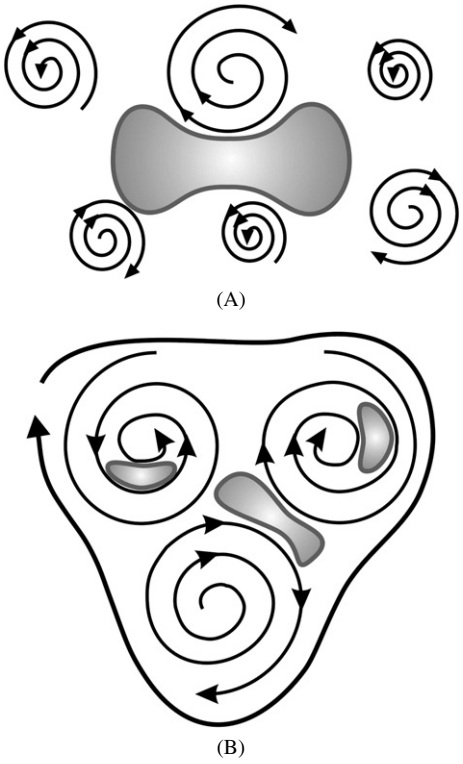

Fig. 1. Schematic presentation of the two regimes of emulsification in turbulent flow. (A) Turbulent inertial regime—the drops are larger than the smallest turbulent eddies and deform under the action of the fluctuations in the hydrodynamic pressure. (B) Turbulent viscous regime—the drops are smaller than the smallest turbulent eddies and, therefore, deform under the action of viscous stress inside and between the eddies.

in the turbulent viscous regime, as compared to the turbulent inertial regime. To the best of our knowledge, this option has not been explored systematically so far. Therefore, one of the major aims of our study is to compare the mean and the maximum drop sizes, after emulsification in these two regimes.

In our previous papers [25–27] we studied the effects of several factors on the mean drop size during emulsification in the inertial turbulent regime, by using the so-called "narrow-gap homogenizer"—see Section 3.2 below for its description and mode of operation. Among the other results, we showed that an equation proposed by Davies [16] describes relatively well the maximum diameter of the stable drops in emulsions, prepared under different hydrodynamic conditions and interfacial tensions, and for oils with viscosity varied between 3 and 100 mPa s [27]. The current study complements our previous work in several aspects. First, we performed experiments with more viscous oils (up to 10,000 mPa s) to check whether the conclusions from the previous studies are still applicable for such viscous oils. Second, the experimental results for the mean drop size and polydispersity of the formed emulsions are compared to theoretical expressions and experimental results of other authors [16–21]. Third, we demonstrate that the emulsification of the viscous oils is much more efficient (smaller drops are formed) when the emulsification is performed at higher viscosity of the aqueous phase and/or at high oil volume fraction. The latter result is explained by analyzing the conditions for

transition from the inertial turbulent regime to the viscous turbulent regime of emulsification.

The paper is organized as follows: Section 2 summarizes the theoretical expressions known from the literature for the maximum drop size and for the drop-size distribution in emulsions, prepared in the two turbulent regimes of emulsification. Section 3 describes the used materials and experimental methods. Section 4 presents the experimental results from the characterization of the hydrodynamic conditions during emulsification. In Section 5, the results from the emulsification experiments in the inertial turbulent regime are presented and compared to theoretical expressions and experimental data by other authors. The results from the emulsification experiments in the viscous turbulent regime are presented in Section 6. Section 7 summarizes the conclusions.

2. Theoretical background

Drops placed in turbulent continuous phase could break upon the action of viscous or inertial stress acting on the drop surface. Which of these stresses dominates depends on the ratio of the drop size and the size of the smallest turbulent eddies in the flow, see Fig. 1. The size of the smallest eddies, λ_0, is given by the so-called "Kolmogorov scale," defined as [12]

$$\lambda_0 \approx \varepsilon^{-1/4}\eta_C^{3/4}\rho_C^{-3/4}, \tag{1}$$

where η_C is the viscosity and ρ_C is the mass density of the continuous phase, while ε is the rate of energy dissipation per unit mass of the fluid (J/kg s), which characterizes the hydrodynamic conditions during emulsification (in reality, there are turbulent eddies with size smaller than λ_0; however, the flow in these eddies is regular and the effect of pressure fluctuations on the drop breakup process is negligible). As seen from Eq. (1), for typical emulsions with $\rho_C \approx 10^3$ kg/m^3, the size of the smallest eddies depends on the viscosity of the continuous phase and intensity of stirring.

According to the Kolmogorov–Hinze theory of emulsification in inertial turbulent regime [12,13], for drops with viscosity comparable to that of water, the maximum stable drop diameter, d_{KH}, can be estimated by comparing the fluctuations of the hydrodynamic pressure in the flow:

$$\langle \Delta P_T(d) \rangle = C_1 \rho_C \langle U^2 \rangle = C_1 C_2 \rho_C (\varepsilon d)^{2/3}, \tag{2}$$

with the capillary pressure of the drops, which opposes the drop deformation:

$$P_C = 4\sigma/d. \tag{3}$$

In Eq. (2), the brackets mean statistical averaging, $\langle U^2 \rangle = C_2(\varepsilon d)^{2/3}$ is the mean square of the fluctuations in the fluid velocity at distance d, and $C_{1,2}$ are numerical constants of the order of unity. From Eqs. (2) and (3), the following expression for d_{KH} was derived [12,13]:

$$d_{KH} = A_1 \varepsilon^{-2/5}\sigma^{3/5}\rho_C^{-3/5} = A_1 d_{KI}, \tag{4}$$

where A_1 is a constant of proportionality of the order of unity, σ is interfacial tension, and d_{KI} denotes the group $(\varepsilon^{-2/5}\sigma^{3/5}\rho_C^{-3/5})$, which has the dimension of length.

In the case of viscous turbulent flow, the drop breakup occurs under the action of the viscous stress, τ_C, inside the smallest turbulent eddies of the continuous phase [12,13] and the maximum stable drop diameter, d_{KV}, can be estimated by comparing τ_C:

$$\tau_C = \eta_C \frac{dU_{\lambda 0}}{dx} \sim \eta_C \frac{(\eta_C \varepsilon/\rho_C)^{1/4}}{\lambda_0} \sim (\varepsilon \rho_C \eta_C)^{1/2}, \tag{5}$$

with the drop capillary pressure, P_C. In Eq. (5), the characteristic velocity inside the smallest eddies, $U_{\lambda 0}$, is found from the comparison of the inertial and viscous stresses for the smallest eddies, $\rho_C(\varepsilon\lambda_0)^{2/3} \sim \eta_C U_{\lambda 0}/\lambda_0$, which leads to $U_{\lambda 0} \sim (\eta_C \varepsilon/\rho_C)^{1/4}$. From Eqs. (3) and (5), the maximum drop size, d_{KV}, is estimated in the viscous regime of emulsification as [12,13,28]

$$d_{KV} = A_2 \varepsilon^{-1/2}\eta_C^{-1/2}\rho_C^{-1/2}\sigma, \tag{6}$$

where $A_2 \approx 4$ is a numerical constant. As seen from Eq. (6), the drop size depends on the viscosity of the continuous phase, η_C, in the viscous regime of emulsification, whereas for the inertial regime of emulsification this dependence is negligible, cf. Eq. (4).

The Kolmogorov–Hinze theory of emulsification does not account explicitly for the influence of the viscosity of the dispersed phase, η_D. Therefore, Eqs. (4)–(6) are valid only for drops with relatively low viscosity, similar to that of water. For such systems, Eq. (4) was experimentally verified by Sprow [14] and further modified in several subsequent studies [15,29–31].

The Kolmogorov–Hinze approach was developed further for more viscous dispersed phase ($\eta_D > \eta_C$) by Davies [16] and Calabrese et al. [18–21]. Davies [16] included the viscous stress inside the deforming drop, $\tau_D \sim [\eta_D \langle U^2 \rangle^{1/2}]/d$ into the total stress balance;

$$\langle \Delta P_T(d) \rangle \approx P_C + \tau_D.$$

Taking into account the known relation $\langle U^2 \rangle = C_2(\varepsilon d)^{2/3}$, one obtains $\tau_D \approx C_2^{1/2}(\eta_D \varepsilon^{1/3} d^{1/3})/d$, and the above stress balance can be expressed as a transcendental equation for the maximum diameter of stable Newtonian drops with viscosity η_D:

$$C_1 C_2 \rho_C (\varepsilon d_D)^{2/3} = 4\sigma/d_D + C_2^{1/2}\eta_D(\varepsilon d_D)^{1/3}/d_D,$$

where C_1 and C_2 are numerical constants defined by Eq. (2). The values $C_1 \approx 0.7$ and $C_2 \approx 2.0$ were calculated by Batchelor in his detailed analysis of turbulent flow [32]. The above equation can be transformed into the following more convenient form:

$$d_D = \left(\frac{4}{C_1 C_2}\right)^{3/5}\left(1 + C_2^{1/2}\frac{\eta_D \varepsilon^{1/3} d_D^{1/3}}{4\sigma}\right)^{3/5}\sigma^{3/5}\rho_C^{-3/5}\varepsilon^{-2/5}$$
$$= A_3\left(1 + A_4\frac{\eta_D \varepsilon^{1/3} d_D^{1/3}}{\sigma}\right)^{3/5} d_{KI}, \tag{7}$$

where A_3 and A_4 are numerical constants, which are expressed through C_1 and C_2. Davies suggested $A_3 \approx 1.0$ and $A_4 \approx 0.35$ as appropriate values for describing the emulsification in the inertial regime [16]. The second term in the parenthesis in the

right-hand side of Eq. (7) expresses the relative contribution of the energy of viscous dissipation, normalized by the surface energy of the deforming drop. At $\eta_D \to 0$ the viscous contribution disappears and Eq. (7) simplifies to Eq. (4). Note that A_3 in Eq. (7) should be equal to A_1 in Eq. (4) to make these equations compatible for oils with low viscosity. Equation (7) was derived under the assumption that the mass densities of the continuous and dispersed phases are similar, $\rho_D \approx \rho_C$.

In a different approach, Calabrese et al. [18–21] compared the energy required for drop deformation with the kinetic energy of the turbulent eddies, for drops containing a Newtonian fluid. The possible difference in the mass densities of the two phases, ρ_D and ρ_C, was considered, and the following generalization of Eq. (7) was derived:

$$d_C = A_5\left(1 + A_6\left(\frac{\rho_C}{\rho_D}\right)^{1/2}\frac{\eta_D\varepsilon^{1/3}d_C^{1/3}}{\sigma}\right)^{3/5} d_{KI}, \tag{8}$$

where $A_5 = 0.054$ and $A_6 = 4.1$ are numerical constants, which Calabrese et al. [19,21] determined by comparing the predictions of Eq. (8) with their experimental data for the mean drop diameter, d_{32}. From the data presented in Ref. [21] we found that Eq. (8) describes also the results for the maximum diameter, d_{V95}, obtained experimentally by Calabrese et al. [19,21], with values $A_5 \approx 0.09$ and $A_6 \approx 3.5$.

Because $\rho_D \approx \rho_C$ in most of the experimental systems, the main difference between the predictions of the models by Davies [16] and Calabrese et al. [18–21] is in the values of the numerical constants A_K. For convenience, we use hereafter A_σ to denote both constants A_3 in Eq. (7) and A_5 in Eq. (8), which are related to the effect of the capillary pressure. Similarly, the notation A_η is used for A_4 in Eq. (7) and A_6 in Eq. (8), which account for the relative effect of drop viscosity. Further discussion of the values of A_σ and A_η, in relation to our experimental results, is presented in Section 5.2 below.

In a third approach, Lagisetty et al. [17] developed and tested a theoretical model for the maximum drop diameter by including the possible effects of the non-Newtonian rheological behavior of the drop phase, and of the time required for drop deformation and breakage. For Newtonian drops (like those in our study) the equations derived by Lagisetty et al. [17] give results, which are numerically similar to those of Calabrese et al. [18] and for this reason will not be reproduced here.

Along with the mean drop diameter, the polydispersity of the drop-size distribution is another important characteristic of the formed emulsions. For emulsions prepared in stirred tanks, Chen and Middleman [15] showed that the drops are normally distributed by volume. Therefore, the following expression was proposed [15] for scaling the experimental data:

$$F_V(d/d_{32}) = 0.5\left[1 + \mathrm{erf}\left(\frac{d/d_{32} - \bar{d}_V/d_{32}}{\sqrt{2}(\sigma_V/d_{32})}\right)\right], \tag{9}$$

where $F_V(x)$ is the cumulative distribution function by volume (derived after integration of the normal distribution function), d_{32} is the mean volume-surface diameter, $\bar{d}_V$ is the mean volume diameter in the normal distribution, and σ_V is the respective standard deviation. Equation (9) was found to describe well a large set of experimental data for emulsions prepared in stirred tanks, with $\bar{d}_V/d_{32} \approx 1.06$ and $\sigma_V/d_{32} \approx 0.24$ [15,18–20]. In a subsequent study performed with static mixer [21], similar data treatment gave $\bar{d}_V/d_{32} \approx 1.12$ and $\sigma_V/d_{32} \approx 0.31$, which shows that the emulsions obtained in the static mixer were more polydisperse than those obtained in the stirred tanks.

In our study we also found that the experimental drop-size distributions by volume are relatively well described by a normal distribution function. To describe the data we use a slightly modified version of Eq. (9), in which the scaling of the drop size is made by the mean volume diameter, d_{V50}, which is experimentally accessible quantity and is an analog of the theoretical mean volume diameter, $\bar{d}_V$ (for perfect normal distribution $d_{V50} \equiv \bar{d}_V$):

$$F_V(d/d_{V50}) = 0.5\left[1 + \mathrm{erf}\left(\frac{d/d_{V50} - \bar{d}_V/d_{V50}}{\sqrt{2}(\sigma_V/d_{V50})}\right)\right]. \tag{10}$$

Equation (10) has the advantage that the ratio $(\bar{d}_V/d_{V50})$ brings direct information about the deviation of the experimentally determined drop-size distribution from the model normal distribution, used to fit the experimental data.

Interestingly, we found that the experimentally determined drop-size distributions by number were better represented by a log–normal distribution function:

$$F_N(d/d_{N50}) = 0.5\left[1 + \mathrm{erf}\left(\frac{\ln(d/d_{N50}) - \ln(\bar{d}_{10}/d_{N50})}{\sqrt{2}\ln(\sigma_{LN})}\right)\right], \tag{11}$$

where $F_N(x)$ is the log–normal cumulative distribution function by number, d_{N50} is the mean number diameter as determined from the experimental data, $\bar{d}_{10}$ is the geometric mean diameter by number in the model log–normal distribution, and σ_{LN} is the respective dimensionless standard deviation, which is defined as the ratio $d(84\%)/d(50\%)$ in the model log–normal distribution [33].

Note that Eqs. (10) and (11) are not strictly compatible with each other, because a perfect log–normal distribution by number corresponds to a log–normal distribution by volume, as well [33], which was not found experimentally. Such qualitatively different experimental distributions by number (closer to log–normal) and by volume (closer to normal) have been reported often in the literature, which shows that this is a rather common situation [18–20].

3. Materials and experimental methods

3.1. Materials

Several surface-active emulsifiers were used to ensure a wide range of oil–water interfacial tensions: nonionic surfactant polyoxyethylene-20 hexadecyl ether (Brij 58, product of Sigma); anionic surfactant sodium dodecyl sulfate (SDS, product of Acros); mixture of the amphoteric surfactant cocoamidopropyl betaine (betaine, product of Goldschmidt Chemical Corporation) with the anionic surfactant sodium dodecylpolyoxyethylene-3 sulfate (SDP3S, product of Stepan Company) in a molar ratio 3:2; and two protein emulsifiers—sodium

caseinate (Na caseinate, commercial name Alanate 180, product of NXMP) and whey protein concentrate (WPC, trade name AMP 8000, product of Proliant). All emulsifiers were used as received. The emulsifier concentration in the aqueous solutions (1 wt% for Brij 58, SDS and betaine + SDP3S, 0.5 wt% for Na caseinate and 3 wt% for WPC) was chosen sufficiently high to suppress drop–drop coalescence during emulsification.

All aqueous solutions were prepared with deionized water, which was purified by a Milli-Q Organex system (Millipore). The aqueous phase contained also NaCl (Merck, analytical grade) with concentration 150 mM for the Brij 58, WPC and Na caseinate solutions, and 10 mM for the SDS solutions. The protein solutions of Na caseinate and WPC contained also 0.01 wt% of the antibacterial agent NaN_3 (Riedel–de Haën). Glycerol (99.5% p.a.) was used to increase the viscosity of the aqueous phase.

As dispersed phase we used several oils of different viscosities: hexadecane with $\eta_D = 3.0$ mPa s (product of Merck); soybean oil with $\eta_D = 50$ mPa s (SBO, commercial product); mineral oils with $\eta_D = 27$ and 147 mPa s (products of Sigma–Aldrich); and seven silicone oils with $\eta_D = 50$, 95, 194, 220, 494, 1024, and 10,000 mPa s (denoted for clarity as SilXX, where XX expresses the oil viscosity). The SBO, mineral oils, and hexadecane were purified from surface-active contaminations by passing the oil through a glass column, filled with Florisil adsorbent [34]. The silicone oils (products of BASF, Rhodia, and TDCS) were used as received.

3.2. Narrow-gap homogenizer

All emulsions were prepared by using a custom-made "narrow-gap" homogenizer with an axially symmetric, cylindrical mixing head [25–27]. The mixing head contained a processing element, through which the oil–water mixture was passed under pressure, see Fig. 2A. Two processing elements were used, both containing annular slits with gap-width of 395 μm and length of 1 mm. The first processing elements had one slit only (Fig. 2B), whereas the second element had two consecutive slits (Fig. 2C).

Oil-in-water emulsions were prepared by applying a two-step procedure. First, two litters of coarse emulsion were prepared by hand-shaking a vessel, containing the necessary amounts of oil and surfactant solution (depending on the desired oil volume fraction Φ in the emulsion). In the second homogenization step, this coarse emulsion was pushed through the narrow-gap homogenizer in a series of consecutive passes. The driving pressure, P, for this step was provided by a gas bottle, containing pressurized nitrogen gas N_2. The driving pressure was controlled during the experiment with a precision of ±500 Pa, with the help of a pressure control system and a pressure transducer mounted close to the homogenizer inlet.

After each pass through the homogenizer, the emulsion was collected in a container attached to the outlet of the equipment, see Fig. 2A. Then the gas pressure in the inlet container was released, and the emulsion was poured back in this container (under the action of gravity), by using a bypass tube. Afterwards, the gas pressure in the inlet container was increased again to the desired value and the emulsion was pushed to make another pass through the homogenizer. 100 consecutive passes of the emulsion through the homogenizer were used to ensure steady-state drop-size distribution, see Fig. 3B.

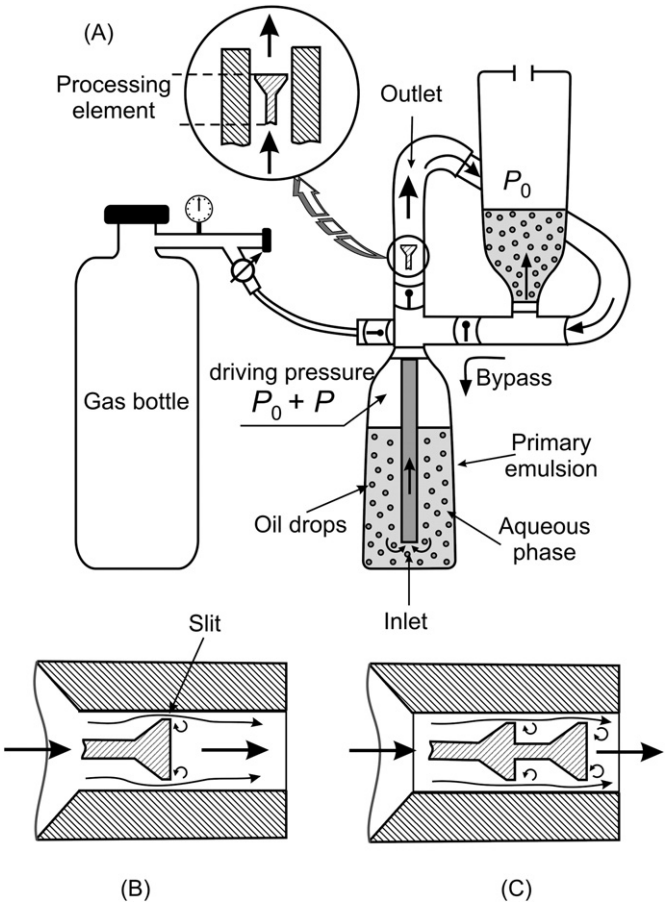

Fig. 2. (A) Schematics of the used homogenizer, which was equipped with cylindrical processing element containing: (B) one annular slit (gap); (C) two consecutive annular slits. An initial oil–water premix was prepared by hand-shaking and introduced in the homogenizer before starting the actual emulsification experiment, as described in Section 3.2. The drop diameters reported in the current paper are measured after 100 passes of the emulsion through the homogenizer to achieve a steady-state drop-size distribution.

3.3. Determination of drop-size distribution

The drop-size distribution in the obtained emulsions was determined by video-enhanced optical microscopy [35,36]. The oil drops were observed and recorded in transmitted light with microscope Axioplan (Zeiss, Germany), equipped with objective Epiplan ×50, and connected to a CCD camera (Sony) and video-recorder (Samsung SV-4000). The diameters of the recorded oil drops were measured one by one, using a custom-made image analysis software, operating with Targa+ graphic board (Truevision, USA). For each sample, the diameters of at least 3000 drops were measured. The accuracy of the optical measurements was estimated to be ±0.3 μm [36].

Two characteristic drop sizes were determined from the measured drop diameters. The mean volume-surface diameter, d_{32},

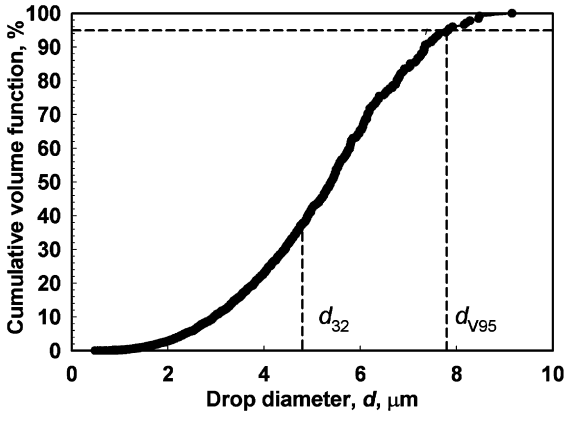

(A)

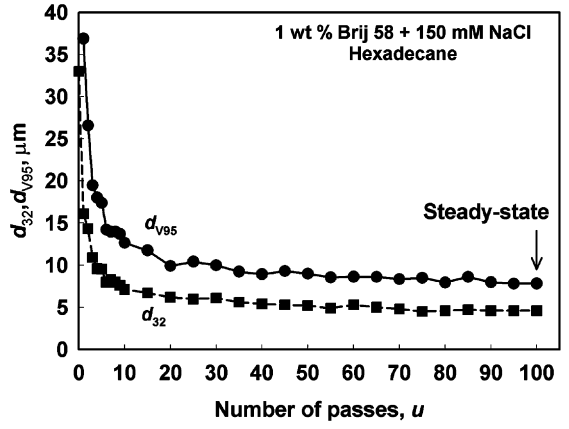

(B)

Fig. 3. (A) Cumulative distribution by volume as a function of drop diameter for hexadecane-in-water emulsion stabilized by 1 wt% Brij 58 + 150 mM NaCl, after 100 passes of the emulsion through the homogenizer. The values of d_{32} and d_{V95} are indicated by dashed vertical lines. (B) The maximum and the mean volume-surface diameters, d_{V95} and d_{32}, for the same system, plotted as functions of the number of passes through the homogenizer.

was calculated from the relation

$$d_{32} = \left(\sum_i N_i d_i^3\right) \Big/ \left(\sum_i N_i d_i^2\right), \tag{12}$$

where N_i is the number of drops with diameter d_i. The volume-95 diameter, d_{V95}, is defined as the diameter, for which 95% by volume of the dispersed oil is contained in drops with $d \leqslant d_{V95}$. The diameter d_{V95} is used as an experimentally accessible measure of the maximum drop size, which is compared in Section 5.1 with the respective theoretical predictions of the drop-breakup models.

3.4. Measurements of oil viscosity and emulsion rheological properties

The viscosity of the oils and of the aqueous solutions was measured at the temperature of the emulsification experiment. The viscosity of soybean oil, hexadecane, and of the aqueous solutions was measured by capillary viscometer, whereas the viscosity of the silicone oils was measured on Gemini research rheometer (Bohlin & Malvern Instruments, UK).

To characterize the rheological properties of the concentrated emulsions with $\Phi \geqslant 0.7$, we used the Gemini rheometer, equipped with parallel-plates of radius 2 cm. Measurements at several gaps were performed (varied between 0.5 and 1 mm) to check for possible effect of the wall-slip, which would compromise the results. The measured rheological properties of the emulsions did not depend on the gap-width in the range of shear rates of interest, between 20 and 3000 s^{-1}, which showed that the possible wall-slip had negligible effect. During these measurements, the emulsion and the parallel plates were closed in a box to reduce water evaporation, which could induce emulsion destruction at the plates' periphery. The reproducibility of the results in consecutive runs was within 10% of the measured stress.

The rheological data from the measurements with the concentrated emulsions were described by the Hershel–Bulkley model [37–39]:

$$\tau(\dot\gamma) = \tau_0 + \tau_V(\dot\gamma) = \tau_0 + c_\eta \dot\gamma^m, \tag{13}$$

where $\dot\gamma$ is the shear rate, τ_0 is the yield stress of the emulsion, τ_V is the respective viscous (shear rate-dependent) stress, m is the power-law index, and c_η is the emulsion consistency.

3.5. Measurement of interfacial tension

The equilibrium oil–water interfacial tension was measured by a drop-shape-analysis of pendant oil drops, immersed in the surfactant solutions. The measurements were performed on commercial Drop Shape Analysis system DSA 10 (Krüss GmbH, Hamburg, Germany).

The dynamic interfacial tension was determined by a recent modification [40] of the stopped jet method [41,42]. Briefly, the method consists in a rapid formation of spherical drop on the tip of a needle, by a sudden stop of continuous jet of one liquid, which is pushed into another liquid. After formation of the drop, the capillary pressure across its spherical surface is measured as a function of time, by using a pressure transducer. From the capillary pressure and the drop radius (measured by a long-focus optical lens) one determines the dynamic surface tension, $\sigma(t)$, starting from times as short as 40 ms. Detailed description of the method is given in Refs. [40–42].

4. Determination of the rate of energy dissipation

For comparison of the experimental data for the maximum and mean drop diameters with the theoretical predictions, Eqs. (4)–(8), one should know the rate of energy dissipation, ε, the interfacial tension, σ, and the viscosities of the dispersed and continuous phases, η_D and η_C. The values of η_D and η_C were determined as described in Section 3.4. The values of σ are discussed in Section 5.1. In a previous study [27], the values of ε were determined by numerical simulations of the turbulent flow for two flow rates of the emulsion ($Q = 0.092$ and 0.145 mL/s), at viscosity of the continuous phase $\eta_C = 1$ mPa s, for both processing elements used (with one and two slits, respectively). In the current study we performed experiments at several additional flow rates and viscosities of the continuous

phase. Therefore, in this section we describe the procedure used for determination of ε under these additional conditions.

First, we measured the dependence of the flow rate, Q, on the driving pressure, P, with the two geometries of the processing element and with aqueous solutions of glycerol, which had different viscosities, $\eta_C = 1.0$, 5.6, and 20 mPa s. The results obtained with pure water, $\eta_C = 1$ mPa s, are shown in Fig. 4A as a dependence $Q(P)$, which is well represented by a power-law empirical fit—see the dashed curves in Fig. 4A. For both geometries of the processing element, this fit is represented by the equation $Q = a_q P^{0.527}$, where $a_{q1} = 0.329$ for the processing element with 1 slit, and $a_{q2} = 0.231$ for the 2-slit processing element (Q is in mL/s, P is in Pa). The relation between P and Q can be represented also by a power-law function, $P = a_p Q^{1.90}$, with $a_{p1} = 8.24$ for the 1-slit geometry and $a_{p2} = 16.22$ for the 2-slit geometry. One sees from these values that $a_{p2} \approx 2a_{p1}$, which shows that the pressure loss is about twice higher for the two-slit processing element at the same flow rate, Q.

The effect of the fluid viscosity, η_C, on the dependence $Q(P)$ was studied for the processing element with two slits. As seen from Fig. 4B, the experimental data for all studied systems could be represented very well by a single master line, when Q is presented as a function of the empirically found group $(P^{0.53}\eta_C^{-0.095})$. The obtained linear relation

$$Q = 0.116 \times P^{0.53}\eta_C^{-0.095} \tag{14}$$

reveals that the dependence of Q on η_C (at fixed P) is very weak in the range between 1 and 20 mPa s, which reflects the turbulent nature of the flow in the homogenizer head (the Reynolds number, $\mathrm{Re} \gg 1$, see Fig. 4C).

The experimental results for the dependence $Q(P)$ could be represented in the form of a friction coefficient, χ, conventionally defined as (see, e.g., Chapter 4 in [43]):

$$\chi = \left(P\frac{H}{L}\right) \Big/ \left(\frac{1}{2}\rho_C U_1^2\right), \tag{15}$$

where H is the gap width (395 μm in our experiments), $L = 1$ or 2 mm is the length of the gaps, and U_1 is the mean linear velocity of the fluid through the gap. The latter can be calculated from the relation $U_1 = Q/S$, where $S = \pi H(D - H)$ is the area of the gap cross-section and D is the external diameter of the annular gap. The respective Reynolds number is defined as $\mathrm{Re} = \rho_C U_1 H_{hyd}/\eta_C$, where $H_{hyd} = 4S/H_P$ and $H_P = [2\pi(D - H)]$ is the wetted perimeter of the gap [27]. The results for the dependence $\chi(\mathrm{Re})$ are summarized in Fig. 4C for all conditions studied. One sees that, at the same Reynolds number, the friction coefficient is the same for the processing elements with one and two slits (see the empty and the full circles in Fig. 4C), which indicates that the higher pressure required to achieve the same flow rate in the 2-slit geometry is due exclusively to the presence of two consecutive slits (with twice longer total length, L) in this geometry. The obtained results are reasonably well described by the semi-empirical relation $\chi = 0.72\mathrm{Re}^{-0.17}$. At high Reynolds numbers, $\mathrm{Re} \geqslant 12{,}000$, the friction coefficient remains almost constant, $\chi = 0.14$, which is around 15 times higher than that for smooth pipes with diameter equal to H and around 3 times lower than the friction coefficient measured for static mixer in Ref. [21]. It should be mentioned that even at relatively low Reynolds numbers, $\mathrm{Re} \approx 500$, the friction coefficient differs significantly from the one characterizing the laminar flow, $\chi = 64/\mathrm{Re}$ [43], which shows that the flow is turbulent in the entire range of emulsification conditions studied. One can conclude from these comparisons that the used narrow-gap homogenizer is a kind of a static mixer, creating turbulent regime of emulsification.

Table 1
Rate of energy dissipation, averaged over the volume of the slit in the processing element, $\bar{\varepsilon}_{gap}$, as found from numerical simulations of the turbulent flow [27]

Re	Q (L/s)	Geometry	$\bar{\varepsilon}_{gap}$ ($m^2\ s^{-3}$)	$P \times 10^{-5}$ (Pa)	$q = V_{DIS}/V_{GAP}$
8450	0.092	One slit	32,706	0.46	15.1
		Two slits	57,490	0.84	15.6
13,250	0.145	One slit	180,247	1.11	10.4
		Two slits	274,308	2.02	12.4

Note. For the two-slit processing element, only the value for the second slit is shown, because this value is higher and governs the maximum drop size in the produced emulsions. Re is the Reynolds number, Q is the emulsion flow rate through the homogenizer, P is the driving pressure, V_{GAP} is the geometrical volume of the narrow slit (gap) in the homogenizer head, and V_{DIS} is the effective volume, in which the main dissipation of turbulent energy takes place (see Section 4 for further explanations).

The hydrodynamic conditions in the homogenizer are characterized by the value of ε, which is a key parameter in the theoretical models of the emulsification process in turbulent flow. In a previous study [27], the values of the gap-averaged turbulent dissipation rate, $\bar{\varepsilon}_{gap}$, was calculated numerically for the 1-slit and 2-slit geometries of the processing element, and at two different flow rates, Q, corresponding to different Reynolds numbers (see Table 1). To find the dissipation rate distribution in the homogenizer, three-dimensional numerical calculations were carried out with Fluent 6.1.22 software package for hydrodynamic calculations. The standard k–ε model, combined with the low-Reynolds-number model for the near-wall region, was used to describe the flow.

To find a reasonable estimate of ε for all conditions used in the current study, we utilized the fact that the rate of energy dissipation, ε, can be approximately assessed by the relation [21]

$$\varepsilon = \frac{PQ}{\rho_C V_{DIS}}, \tag{16}$$

where V_{DIS} is the effective volume, in which the main turbulent dissipation of energy takes place, whereas P and Q are the respective pressure and flow rate during the experiment. Therefore, if an estimate of V_{DIS} is available, one could find ε from Eq. (16) and the known values of P and Q.

From the numerical calculations performed in Ref. [27], we could estimate the ratio $q = V_{DIS}/V_{GAP}$, where $V_{GAP} = 8.6 \times 10^{-9}\ m^3$ is the geometrical volume of one gap (slit) in the processing element. One sees from Table 1 that q is almost the same for both studied processing elements when the Reynolds numbers are similar. However, the value of q decreases by about 50% with the increase of the Reynolds number, Re, from 8450

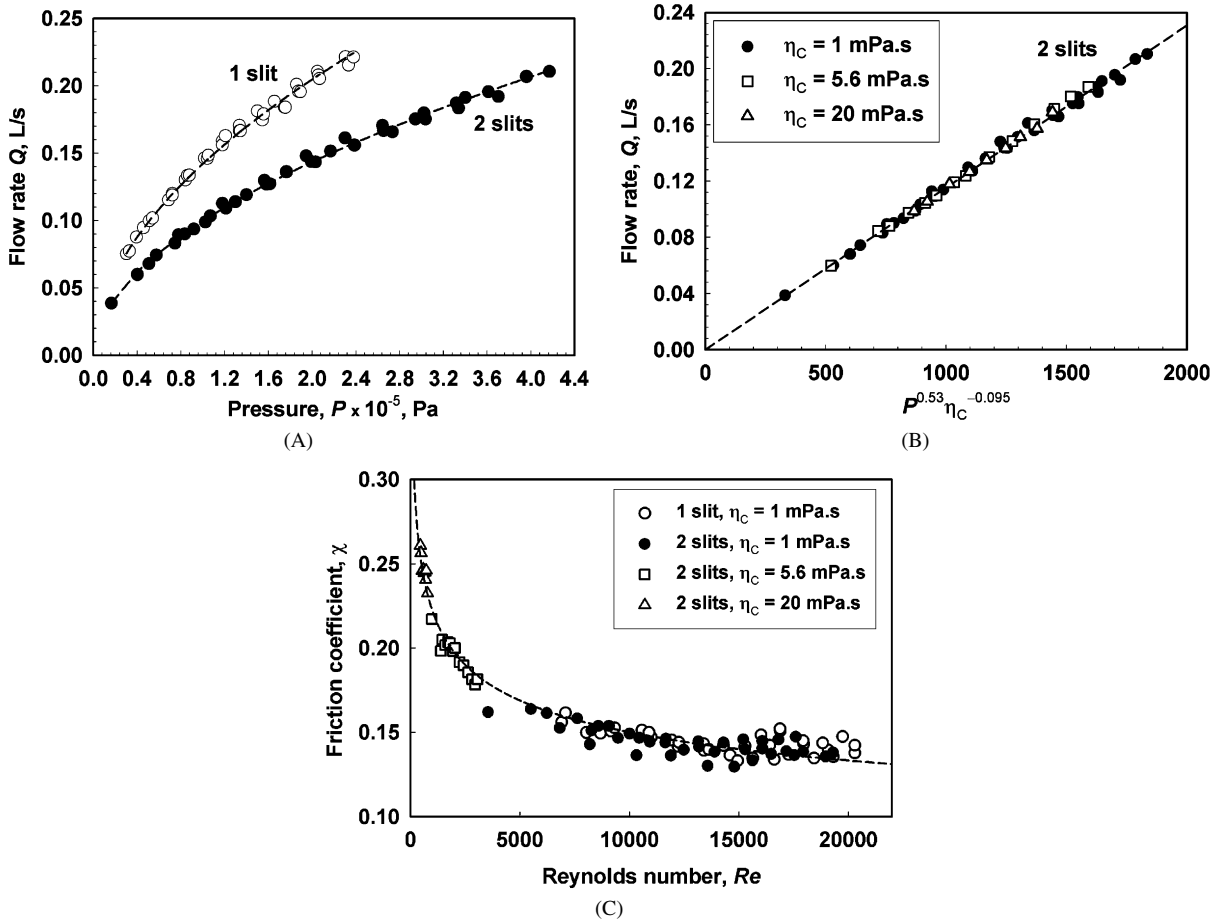

Fig. 4. (A) Flow rate, Q, vs the applied pressure, P, for the processing elements with 1 slit (open circles) and with 2 slits (full circles). (B) Q vs $(P^{0.53}\eta_C^{-0.095})$ for the processing element with 2 slits, at three different viscosities of the aqueous phase, η_C. (C) Friction coefficient, χ, defined by Eq. (15), as a function of the Reynolds number, Re. The points are experimental data, whereas the dashed curve is a power-law fit to these data, $\chi = 0.72\mathrm{Re}^{-0.17}$.

to 13,250. Assuming as an approximation that the dissipation volume depends linearly on the Reynolds number (in the range of ε-values used in the current study), we could fit the data from Table 1, for the processing element with 2 slits, by the equation $q = (21.24 - 6.7 \times 10^{-4}\mathrm{Re})$. Thus we obtained the following approximate estimate:

$$\varepsilon = \frac{PQ}{(21.2 - 6.67 \times 10^{-4}\mathrm{Re})\rho_C V_{GAP}}. \qquad (16')$$

To check the applicability of Eq. (16′) to describe the systems under investigation, we performed three series of control emulsification experiments with hexadecane as oil phase, and Brij 58, WPC and Na caseinate as emulsifiers. The Reynolds number was varied between 6420 and 19,300, to cover the entire range of energy dissipation rates, ε, used in the current study. The experimental results for the maximum stable drop diameter, d_{V95}, are plotted in Fig. 5 as a function of the group $(\varepsilon^{-2/5}\sigma^{3/5}\rho_C^{-3/5})$, see Eq. (4), by using for ε the values estimated from Eq. (16′). The interfacial tensions entering Eq. (4) were measured to be $\sigma = 7.0$, 28.5, and 28.8 mN/m for Brij 58, WPC, and Na caseinate-stabilized emulsions, respectively (see Section 5.1 for explanations about these values). One sees from Fig. 5 that the experimental values of d_{V95} for all emulsions fall on a straight line, in agreement with Eq. (4), which indicates that the values of ε used to construct the plot are properly approximated by Eq. (16′). Note, that Eq. (16′) is supported also by the numerical calculations of ε performed in Ref. [27].

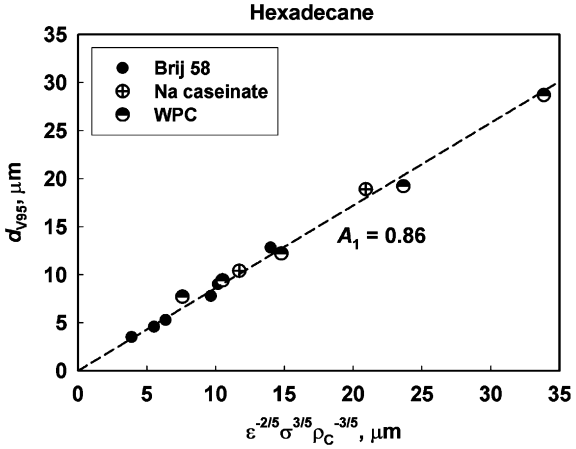

Fig. 5. Experimental values of d_{V95} plotted vs $(\varepsilon^{-2/5}\sigma^{3/5}\rho_C^{-3/5})$, see Eq. (4), for hexadecane-in-water emulsions. From the slope of the best linear fit (dashed line) one determines the constant $A_1 = 0.86$. The emulsions are prepared with three different emulsifiers and at several flow rates, Q, which correspond to different Reynolds numbers, Re, and different rates of energy dissipation, ε (see the text for further explanations).

The slope of the straight line in Fig. 5 gives the value of $A_1 = A_3 \approx 0.86$ (see Eqs. (4) and (7)), which is very close to the value $A_3 \approx 1.0$, suggested by Davies [16]. In the following Section 5, the value $A_3 = 0.86$ is shown to describe satisfactorily all results obtained with the various systems studied (including those with the more viscous oils).

5. Inertial turbulent regime of emulsification

In the current section we compare our experimental results for the maximum drop diameter, d_{V95}, with the respective theoretical expressions for the inertial turbulent regime of emulsification, see Eqs. (7) and (8). Particular attention is paid to the values of the numerical constants, A_K, entering these expressions to clarify which set of values ensures satisfactorily description of the experimental data.

5.1. Experimental results and their comparison with theoretical models

In Ref. [27] we studied the effects of the energy dissipation rate, number of slits in the processing element, equilibrium interfacial tension, and viscosity of the oil phase (varied between 3 and 100 mPa s) on the maximum drop size, d_{V95}. The results were described with Eq. (7), by taking the literature value $A_4 \approx 0.35$, and considering A_3 as adjustable parameter. The least-squares method gave $A_3 = 0.86$ and a mean-square relative error of 12.5% [27]. A close look on the comparison between the experimental data and the theoretical prediction evidences, however, a not very large, but systematic deviation for the emulsions prepared with the protein Na caseinate—the experimental drop size was somewhat larger than predicted (see Fig. 9 in Ref. [27]).

To clarify the possible reasons for this discrepancy, in the current study we performed additional experiments. Emulsification experiments with another protein sample (whey protein concentrate, WPC) showed similar systematic deviations when using the equilibrium interfacial tension in the theoretical estimates of d_D. Interestingly, we found by direct numerical checks that, if we use the interfacial tension of the pure oil–water interface in the estimates for the protein-stabilized samples (instead of the equilibrium interfacial tensions), we obtain better agreement of the data with the theoretical predictions of d_D. These results indicate that the protein adsorption is probably too slow to justify the use of the equilibrium interfacial tension for description of the emulsification process in protein systems. Therefore, we tested the use of the dynamic interfacial tensions of the protein solutions, as determined by the stopped jet method [40–42], to estimate d_D by Eq. (7). The dynamic tension at the shortest achievable time in the stopped jet method, $t = 40$ ms, was used in these estimates. The numerical checks showed that the agreement between the experimental data and the predictions of Eq. (7) is better for all protein-stabilized emulsions studied, when σ ($t = 40$ ms) is used to calculate d_D. Therefore, the dynamic interfacial tensions for the protein solutions and the equilibrium interfacial tensions for the low molecular mass surfactants (which gave better agreement) are used in the following consideration.

According to Eq. (7), the experimental data for the various systems should fall on a master line, when plotted as $(d/d_{KI})^{5/3}$ versus $\eta_D(\varepsilon d)^{1/3}/\sigma$. The respective dependences for d_{V95} and d_{32} are presented in Figs. 6A and 6B, respectively, for hexadecane with $\eta_D = 3$ mPa s, mineral oil with $\eta_D = 27$ mPa s, soybean oil with $\eta_D = 50$ mPa s, and silicone oils with $\eta_D = 50$ and 95 mPa s. Emulsions stabilized with different surfactants were studied to ensure a wide range of interfacial tensions, varying between 4.8 and 28.8 mN/m (see Table S1 in Supplementary material attached to this paper). As seen from Fig. 6A, the experimental data for all systems follow a linear dependence, which was plotted by using the value of $A_3 = A_1 = 0.86$ as obtained with the hexadecane samples (Fig. 5) and $A_4 = 0.37$, which was determined from the best fit to the data for all oils included in this figure. The respective correlation coefficient is $r^2 = 0.93$. The data for d_{32} were also described rather well by a linear dependence for all oils with $\eta_D < 100$ mPa s, by using the values $A_3 = 0.56$ and $A_4 = 0.23$ ($r^2 = 0.96$, Fig. 6B). The difference between the values of A_3 for d_{V95} and d_{32} reflects the fact that the mean volume-surface diameter is about twice smaller than the maximum diameter at low viscosity of the oil, $d_{32}/d_{V95} \approx 0.6$. The lower value of A_4 for d_{32} indicates different relative contributions of the viscous friction into d_{V95} and d_{32}, which is related also to the observed higher polydispersity of the emulsions prepared with more viscous oils (see below for discussion of polydispersity).

We tested the values of A_3 and A_4, obtained as described above, with systems having higher viscosity of the dispersed phase, $100 < \eta_D < 500$ mPa s. The experimental data for five emulsions—four of them obtained with silicone oils with $\eta_D =$ 194, 220, and 494 mPa s, and another emulsion obtained with mineral oil with $\eta_D = 147$ mPa s, were added to the plot $(d/d_{KI})^{5/3}$ versus $\eta_D(\varepsilon d)^{1/3}/\sigma$, see Figs. 6C and 6D. As seen from Fig. 6C, the data for the maximum stable diameter, d_{V95}, in the emulsions with $\eta_D = 147$, 194, and 220 mPa s fall relatively well on the predicted line. For the most viscous oil with $\eta_D = 494$ mPa s (denoted as Sil500 in Fig. 6), the deviation is already significant (by ≈25%). On the other hand, Fig. 6D shows that for all viscous oils with $\eta_D > 150$ mPa s, the discrepancy between the measured values of d_{32} and the estimated linear dependence is significant and rapidly increases with oil viscosity. One can conclude from these results that the linear dependence defined by Eq. (7) is satisfied in significantly wider range of oil viscosities for d_{V95}, as compared to d_{32}.

The latter experimental result is in agreement with the presumption that Eqs. (7) and (8) are derived for the maximum diameter of the stable drops (represented better by d_{V95}) rather than for the mean diameter d_{32}. This difference is insignificant for emulsions with fixed drop polydispersity, for which the ratio d_{V95}/d_{32} remains constant and, subsequently, the two plots would be linear in the same range of governing parameters. However, if the emulsions have different polydispersities, the ratio d_{V95}/d_{32} changes, and the linear dependence presented by Eq. (7) cannot be simultaneously satisfied for both d_{V95} and d_{32}. Indeed, the examination of our experimental results

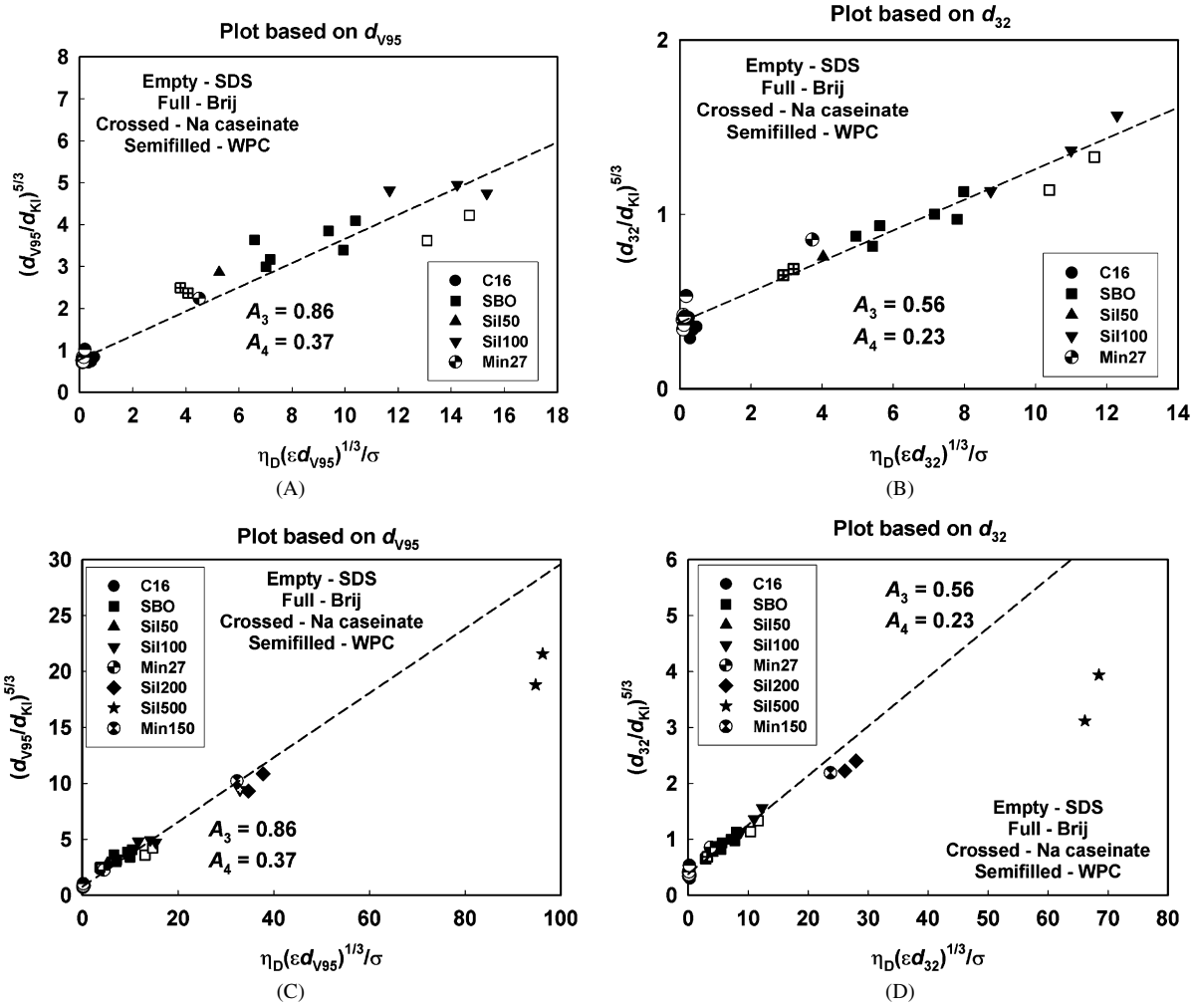

Fig. 6. (A, B) Plots of $(d/d_{KI})^{5/3}$ as a function of $\eta_D(\varepsilon d)^{1/3}/\sigma$ for 27 emulsions with $3.0 \leqslant \eta_D \leqslant 95$ mPa s. (A) and (B) correspond to $d = d_{V95}$ and $d = d_{32}$, respectively. The symbols are experimental data, whereas the dashed lines represent best linear fits, according to Eq. (7). (C, D) Similar plots including 32 emulsions with $3.0 \leqslant \eta_D \leqslant 494$ mPa s. The dashed lines are drawn to be the same as in (A) and (B).

showed that the emulsions obtained with more viscous oils were significantly more polydisperse than those obtained with oils of lower viscosity, see Table S1.

Fig. 7 presents the correlation plot between the theoretically predicted values of the maximum stable drop diameters, d_D, calculated from Eq. (7) with $A_3 = 0.86$ and $A_4 = 0.37$, and the corresponding experimentally measured diameters, d_{V95}, for all emulsions studied. As seen from Fig. 7, the correlation is relatively good in a wide range of oil viscosities ($3 \leqslant \eta_D < 500$ mPa s), interfacial tensions ($5 \leqslant \sigma \leqslant 28$ mN/m), energy dissipation rates ($2.2 \times 10^4 \leqslant \varepsilon \leqslant 9.6 \times 10^5$ J/kg s) and for the two geometries of the processing element used. The average relative error is ≈8%. Therefore, the theoretical model, Eq. (7), with $A_3 = 0.86$ and $A_4 = 0.37$, predicts rather well the effects on the maximum drop diameter, d_{V95}, of all factors studied.

The effects of the studied factors on the polydispersities of the emulsions are illustrated in Fig. 8 (see also Table S1). According to Eq. (10), the volume distribution of different emulsions with similar polydispersity should fall on a master curve, when the cumulative distribution F_V is plotted as a function of the scaled drop diameter, d/d_{V50}. We found that the experimental data for the drop-size distribution fall on a master curve, when the emulsions are prepared with oils of similar viscosities, see Fig. 8A. In other words, the emulsion polydispersity varied only slightly with the changes in the interfacial tension and

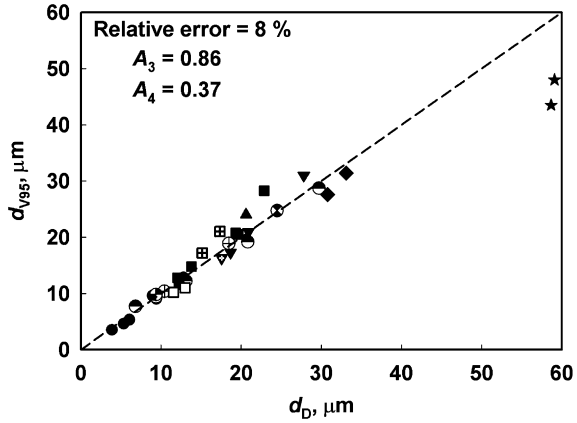

Fig. 7. Correlation plot for the theoretically predicted values of the maximum drop diameter, d_D (see Eq. (7)), and the corresponding experimental values, d_{V95}. The symbols correspond to different systems, as described in Fig. 6.

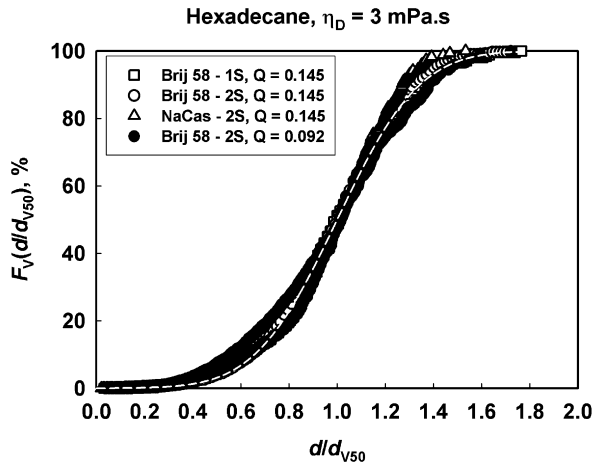

Fig. 8. (A) Cumulative distribution by volume, F_V, versus the scaled drop diameter, d/d_{V50}, for hexadecane. The points are experimental data for emulsions prepared under different conditions as indicated in the legend, whereas the dashed curve is the best fit by normal distribution function, Eq. (10). In the legend, Q is the flow rate in L/s, whereas 1S and 2S indicate the processing elements with 1 and 2 slits, respectively. (B) Comparison of the best fits of the cumulative volume functions, F_V, for oils with different viscosities, versus the scaled drop diameter, $d/\overline{d}_V$.

the rate of energy dissipation during emulsification. However, the distributions for emulsions obtained with oils of different viscosities were rather different from each other—see the comparison in Fig. 8B. As one can see from the data shown in Table S1, the scaled polydispersity of the emulsions, σ_V/d_{V50}, significantly increased with the increase of oil viscosity. These results are further discussed in the following subsection.

5.2. Comparison of our results with the results by other authors

The values of the numerical constants $A_3 = A_\sigma$ and $A_4 = A_\eta$ obtained by interpreting our data with Eq. (7) are compared in Table 2 with the values of the same constants, as determined by other authors. For comparison, we show also the type of the used emulsifying device and the ranges of dispersed phase viscosities and interfacial tensions, explored by the different authors.

One sees that the values of A_σ and A_η obtained in the current study are in a very good agreement with those presented in the papers by Davies [16] and Hinze [13], and substantially differ from those reported in Refs. [14,18–20]. The values of A_σ reported in Refs. [18–20] are much smaller than those found in our study and in Refs. [13,16], whereas the opposite trend is observed for the values of A_η. Note that the value of A_η accounts for the relative contribution of the viscous friction in the drop breakup process, so that the actual value of this constant brings a non-trivial physicochemical information.

The discrepancy noticed above arises most probably from the different expressions used to estimate the rate of energy dissipation in the emulsification devices. The values reported in Refs. [14,18–20] were obtained with impeller devices, and the respective average values of ε were used to construct linear plots similar to those shown in Fig. 6 and to determine the values of A_σ and A_η. On the other hand, the average values of ε in the impeller devices were shown to be about two orders of magnitude smaller than the maximum values of ε, which are realized in the regions close to the impeller tips, where the stirring is most intensive [3,44]. One could expect that after a sufficiently long period of emulsification, when the steady-state drop-size distribution is achieved, the maximum drop size should be governed mainly by the regions with highest rate of energy dissipation, rather than by regions characterized with the average values of ε. Our numerical checks showed that, if the maximum values of ε ($\approx$80 times higher than the average ones [3,44]) are used to fit the same set of experimental data, the values of A_σ and A_η corresponding to $\approx$0.09 and $\approx$3.5 for d_{V95} in impeller devices [18–20] become equal to $\approx$0.5 and $\approx$0.9, respectively, i.e. much closer to the values determined in our study and with static mixer in Ref. [21]—see Fig. 9 for illustration of this effect of ε on the estimated values of A_σ and A_η.

Summarizing, we suppose that the main reason for the large differences in the values of A_3 and A_4, reported by various authors, is due mainly to the specific definition of ε, which is used to construct the linear plots in the studies with impellers. Note that by unifying the definitions of ε for the various emulsification devices (e.g., by using the rate of energy dissipation in the "most active" zones of the impeller type homogenizers), one would be able to predict better the results from emulsification of a given system in the various devices.

To the end of this subsection, we discuss briefly the results about the emulsion polydispersity. As explained in Section 5.1, we could not describe our experimental data by a single master curve for the oils with different viscosities (which was the case with the experimental results described by Calabrese et al. [18–21] for the oils falling in the same viscosity range). This result is related to the fact that the oils with higher viscosity resulted in more polydisperse emulsions in our experiments, whereas the polydispersities of all emulsions were very similar in Refs. [18–21]. This difference is probably due to the fact that the drop-size distributions in our systems are strongly affected by the small daughter drops (called also in the literature "satellite drops"), which form during emulsification and have diameters much smaller than d_K and d_D. Indeed, the typical mean drop size in our experiments was of the order of mi-

Table 2
Values of the constants A_σ and A_η (see Eq. (7) and the paragraph after Eq. (8)), as determined by various authors to describe the drop breakup in inertial turbulent regime of emulsification

Study	Homogenizer type	Viscosity range (mPa s)	Interfacial tension (mN/m)	A_σ	A_η
Davies [16]		Theoretical expression		≈1.0	≈0.35[a]
Sprow [14]	Impellers	0.51	41.8	0.138	Not defined
Calabrese et al. [18–20]	Impellers	5 to 500	1 to 45	≈0.09	≈3.5
Berkman and Calabrese [21]	Static mixer	0.6 to 200	31.8 to 41.6	0.416	1.47
Hinze [13]	Coaxial cylinders	Low	Not defined	0.725	Not defined
Current study	Narrow-gap homogenizer	3 to 500	≈5 to 30	0.86	0.37

[a] Calculated by us, following the approach from Ref. [16] and by using the numerical constants C_1 and C_2 determined by Batchelor [32].

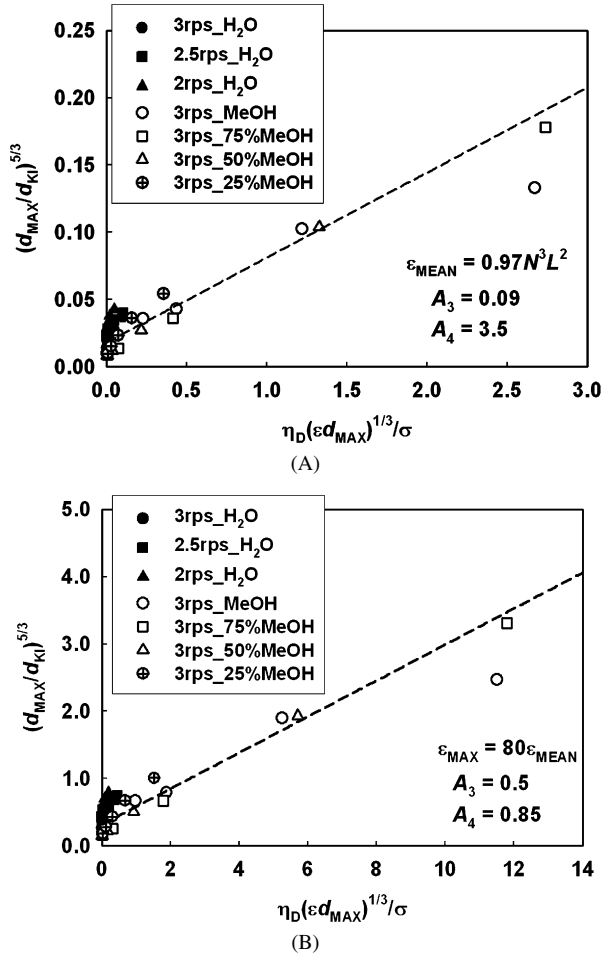

Fig. 9. Plot of $(d/d_{KI})^{5/3}$ as a function of $\eta_D(\varepsilon d)^{1/3}/\sigma$, with experimental data from Ref. [19] obtained with impellers ($1.0 \leqslant \eta_D \leqslant 500$ mPa s, $1.0 \leqslant \sigma \leqslant 45$ mN/m): (A) based on the mean value of the power dissipation rate, $\varepsilon_{MEAN} = 0.97N^3L^2$ (Eq. (11) in Ref. [18]), where N is impeller speed and L is impeller diameter; (B) based on the maximal value of the power dissipation rate, $\varepsilon_{MAX} \approx 80\varepsilon_{MEAN}$. The symbols represent experimental data for $d_{MAX} \approx d_{32}/0.6$ [19], whereas the lines represent fits by Eq. (8), with values of A_σ and A_η as shown in the graphs.

crometers and was strongly affected by the contribution of the satellite drops, which have comparable sizes. In contrast, the typical mean drop size in the emulsions studied by Calabrese et al. [18–21] was above 100 μm, which suggests that the satellite drops (probably of micrometer size) had negligible contribution into the volume size distributions, presented and discussed in Refs. [18–21].

The contribution of the satellite drops in our systems was particularly important in the size distributions by number. These distributions were better represented by the log–normal model function (as compared to the normal distribution), and the mean number diameter, d_{N50}, was determined mainly by the size of satellite drops with diameters well below d_D. As seen from Table S1, the only clear effect of the various factors on d_{N50} was the larger values, observed with the protein solutions of Na caseinate and WPC, which had rather high interfacial tensions. On the other hand, the polydispersity in the number distributions increased significantly with the increase of both the interfacial tension and oil viscosity, see Table S1 and Fig. S2 for examples. These results are further discussed in our subsequent study [8].

6. Emulsification in turbulent viscous regime

According to Kolmogorov theory [12], the increase of the viscosity of the aqueous phase, η_C, leads to increase of the size of the smallest turbulent eddies, λ_0 (see Eq. (1)). As a result, the emulsified drops could become smaller than λ_0 and the emulsification would occur in the viscous regime (see Eq. (6) and Fig. 1). The effect of the emulsification regime (inertial turbulent or viscous turbulent) on the drop size is explored in the current section.

6.1. Effect of the viscosity of the aqueous phase, η_C

The effect of η_C on the drop-size distribution was studied with diluted emulsions, $\Phi = 0.01$, of silicone oil with viscosity 95 mPa s. To ensure high emulsion stability (especially needed at the higher oil volume fractions discussed in the following Section 6.2), we used the surfactant mixture of betaine and SDP3S, with 1 wt% total concentration and 3:2 molar ratio. To increase the viscosity of the aqueous phase, we added glycerol with concentration varied between 0 and 70 wt%, which corresponded to variations of η_C between 1 and 18 mPa s.

The experimental results showed that the maximum size of the drops, d_{V95}, decreased almost 3 times (from 17 to 6 μm), while increasing η_C from 1 to 18 mPa s, see Fig. 10. Note that the increase of the driving pressure, P, needed to achieve the smaller drop size in these emulsions, was relatively small (by ≈30% only), due to the very weak dependence of P on η_C, see Eq. (14).

To clarify the type of the emulsification regime realized at the various viscosities of the aqueous phase, we calculated the maximum drop diameter, d_D, as predicted by Eq. (7)

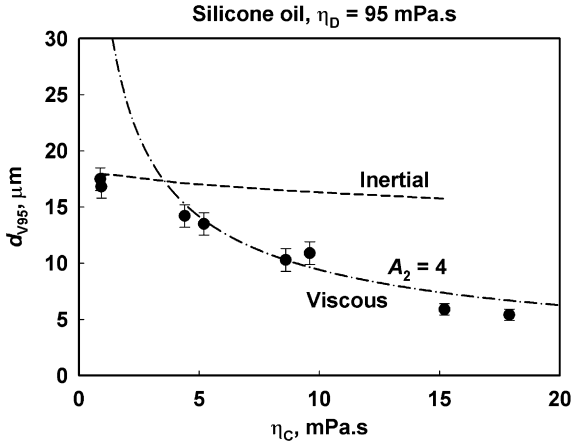

Fig. 10. Maximum drop diameter, d_{V95}, as a function of the viscosity of the aqueous phase, η_C, for emulsions of silicone oil with $\eta_D = 95$ mPa s, stabilized by 1 wt% betaine + SDP3S (molar ratio 3:2) + glycerol of different concentrations. The two curves show the theoretical predictions for the maximum drop diameter in the inertial regime, d_D, and in the viscous turbulent regime, d_{KV} (see Eqs. (7) and (6), respectively).

with $A_3 = 0.86$ and $A_4 = 0.37$, and compared this theoretical prediction to the experimentally measured values of d_{V95}. A significant discrepancy is observed between the theoretically predicted and the experimentally measured values (the ratio $d_D/d_{V95} > 1$), when the viscosity η_C becomes higher than ca. 3 mPa s. The facts that (i) the drop size decreases with the viscosity of the continuous phase and (ii) Eq. (7) derived for the inertial regime of emulsification does not describe the drop size at $\eta_C > 3$ mPa s, indicate that the regime of emulsification changed from turbulent inertial into turbulent viscous at higher viscosity of the aqueous phase, cf. Eqs. (6) and (7). To check further this hypothesis, we estimated the size of the smallest turbulent eddies, λ_0, by Eq. (1) and found that a significant deviation from the theoretical dependence for the inertial regime of emulsification is observed when the drop diameter, d_{32}, becomes comparable to λ_0 (see Table S2).

Thus we can conclude that the drop breakup in emulsions with $\eta_C > 3$ mPa s occurs in the viscous turbulent regime, for which the maximum stable diameter is given by Eq. (6). Using the values of ε from Eq. (16′), and the experimental values of η_C and σ, we could compare the theoretically predicted d_{KV} from Eq. (6) with the experimental values of d_{V95}. This comparison showed that $d_{KV} \approx d_{V95}$, if $A_2 \approx 4$ (see Fig. 10), which is a very reasonable value. Indeed, if we equilibrate the capillary pressure of the oil drops, $P_C = 4\sigma/d$, with the viscous stress in the smallest eddies, Eq. (5), we obtain the theoretical estimate $A_2 \approx 4$, which agrees perfectly with the experimental results. However, one should note that from hydrodynamic viewpoint A_2 is an analog of the critical number for drop breakup in shear flows and, therefore, A_2 is expected to depend on the viscosity ratio η_D/η_C. More experimental data are needed to check whether Eq. (6), with appropriately chosen values of A_2, could describe adequately the maximum drop diameter in the viscous turbulent regime for a wider range of systems.

The experimental data for the drop-size distribution by volume, F_V, as a function of the scaled drop diameter, d/d_{V50}, are compared in Fig. S3 for different viscosities of the aqueous phase. The drops are reasonably well described by normal distribution function. The dimensional polydispersity of the drops, σ_V, was found to decrease, whereas the scaled polydispersity, σ_V/d_{V50}, increased (due to the faster decrease of d_{V50}) with the increase of the viscosity of the aqueous phase, η_C, see Table S2.

In conclusion, a transition from inertial into viscous regime of emulsification in turbulent flow could be accomplished by a moderate increase of the viscosity of the aqueous phase, which results in smaller mean and maximum drop diameters. Since the hydrodynamic resistance of the used narrow-gap homogenizer (which is a kind of static mixer) depends only slightly on the viscosity of the aqueous phase in the case of turbulent flow, see Fig. 4B, this is an appropriate procedure for obtaining finely dispersed emulsion droplets.

6.2. *Effect of the oil volume fraction, Φ*

The effect of Φ was studied for emulsions of silicone oils with viscosities of 100, 1000, and 10,000 mPa s. The surfactant mixture betaine + SDP3S in molar ratio 3:2 was used to stabilize the drops against coalescence. In the emulsions with oil volume fraction varied between $\Phi = 0.01$ and 0.2, the total surfactant concentration was 1 wt% (defined with respect to the aqueous phase in the emulsion). In the emulsions with $\Phi = 0.5$, the total surfactant concentration was 2.5 wt%, and in the emulsions with $\Phi = 0.7$ and 0.8 the surfactant concentration was 5.8 wt%. These higher concentrations were chosen to ensure sufficient surfactant in the emulsion, which was able to cover the surface of drops of mean diameter as small as $d_{32} \approx 1$ μm, with adsorption layer of at least $\Gamma = 2.5$ mg/m^2, thus avoiding the possible surfactant depletion from the aqueous phase during the emulsification process (for estimate of the effect of surfactant adsorption on the bulk surfactant concentration see Eq. (4) in Ref. [26]).

The experimental results for $d_{V95}(\Phi)$ and $d_{32}(\Phi)$ are shown in Fig. 11. For all oils, the maximum and the mean drop diameters change only slightly upon the initial increase of Φ from 0.01 to ca. 0.5. The further increase of Φ causes a sharp decrease of d_{V95} and d_{32}. Furthermore, the microscope observations revealed that the increase of Φ above 0.6 led to decrease of emulsion polydispersity (see Table S3). This effect was more pronounced for the emulsions of the more viscous oil, which were very polydisperse at low volume fractions, see Fig. 12 (see also the discussion in Section 5.5 of the third part of this series [8]). Similar decrease of the mean drop size and of the emulsion polydispersity upon increase of Φ were reported previously in the literature [45–47], without giving an explicit explanation for the observed trends. The sharp change in the emulsion characteristics upon the increase of Φ above 0.6 indicates a possible change in the regime of emulsification when concentrated emulsion is passed through the homogenizer. In the following, we suggest a plausible explanation of these results.

Following our discussion from the previous Section 6.1, we suppose that the observed decrease of the mean drop size at high oil volume fraction ($\Phi > 0.6$) is related to the increased vis-

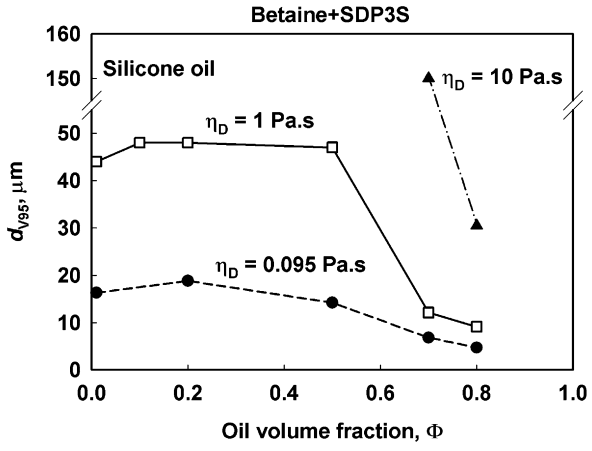

(A)

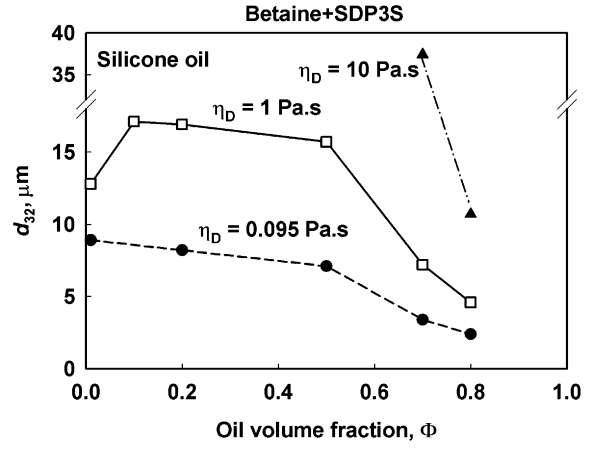

(B)

Fig. 11. (A) Maximum drop diameter by volume, d_{V95}, and (B) mean volume-surface diameter, d_{32}, as functions of the oil volume fraction, Φ, for emulsions of silicone oil with $\eta_D = 95$ mPa s (circles), $\eta_D = 1024$ mPa s (squares), and $\eta_D = 10{,}000$ mPa s (triangles) stabilized by betaine + SDP3S (molar ratio 3:2).

cosity of the concentrated emulsions, which induces a change of the emulsification regime from turbulent inertial to turbulent viscous. To check this hypothesis we characterized the rheological properties of the concentrated emulsions with $\Phi = 0.7$ and 0.8, of three silicone oils ($\eta_D \approx 100$, 1000, and 10,000 mPa s). The dependence of the shear stress on the shear rate, $\tau(\dot\gamma)$, was measured as described in Section 3.4 and the Hershel–Bulkley model was used to fit the data and to determine the yield stress, τ_0, the consistency, c_η and the power-law index, m, of these emulsions, see Table 3. As expected, the yield stress, τ_0, increased with the increase of Φ and with the decrease of the mean drop size [37,48]. For all studied emulsions, the contribution of τ_0 to the total shear stress was negligible for the relatively high shear rates, which are realized in the homogenizer head, $\dot\gamma > 10^4\ \mathrm{s}^{-1}$ (see below for the respective estimate). Therefore, the contribution of τ_0 is neglected in the following discussion and the emulsions are described as power-law fluids.

To estimate the mean drop size in concentrated emulsions, subject to turbulent flow, we should modify Eqs. (1) and (6) to account for the non-Newtonian rheological behavior of these emulsions. Following the reasoning of Kolmogorov [12,43], we

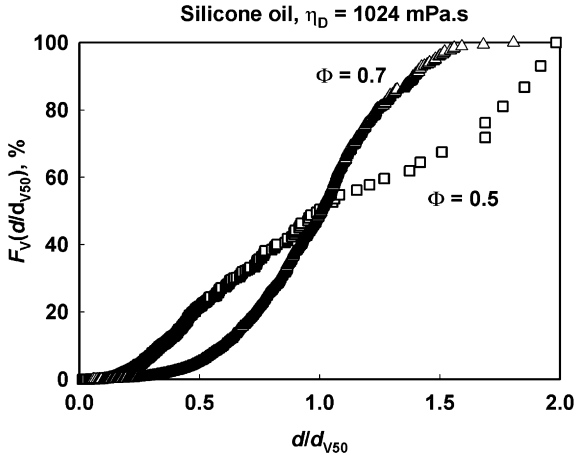

Fig. 12. Cumulative volume distribution, F_V, as a function of the scaled drop diameter, d/d_{V50}, for emulsions of silicone oil with viscosity 1024 mPa s, prepared at two oil volume fractions, Φ.

could estimate the size of the smallest eddies in the flow, λ_0, by assuming equal magnitude of the fluctuations in the dynamic pressure, $\langle \Delta P_T \rangle$, and the viscous stress, τ_C, for these eddies:

$$\langle \Delta P_T \rangle \approx \tau_C \quad \Rightarrow \quad \rho_C U_\lambda^2 \sim \rho_C (\varepsilon \lambda_0)^{2/3} \approx c_\eta \dot\gamma^m \sim c_\eta \left[\frac{(\varepsilon\lambda_0)^{1/3}}{\lambda_0} \right]^m. \tag{17}$$

From Eq. (17), the following expression for λ_0 is obtained in the case of a power-law fluid:

$$\lambda_0 = \left(\frac{c_\eta}{\rho_C} \right)^{3/(2(1+m))} \varepsilon^{(m-2)/(2(1+m))}, \tag{18}$$

which reduces to Eq. (1) upon setting $m = 1$. Next, by assuming comparable average viscous stress in the emulsion and capillary pressure of the drops, we obtain an analog of Eq. (6) for the maximum diameter of the stable drops in a concentrated emulsion, characterized as a power-law fluid:

$$d_{V,PL} = A_7 \sigma c_\eta^{-1/(m+1)} (\varepsilon \rho_C)^{-m/(m+1)}, \tag{19}$$

power-law emulsion viscous turbulent regime of emulsification.

Here A_7 is unknown constant, which could depend on the viscosity of the dispersed phase (it plays the role of the critical capillary number leading to drop breakage in shear flow).

From the experimentally measured values of c_η and σ, and from the values of ε calculated from Eq. (16′), we could estimate the maximum diameter of the stable drops from Eq. (19) and compare it with the experimental values of d_{V95}. In this way we could determine the value of A_7 for the various concentrated emulsions studied. The obtained results for A_7 are plotted in Fig. 13 as a function of the viscosity ratio, η_D/η_{EM}, where η_{EM} is the effective viscosity of the emulsion at shear rate, $\dot\gamma \approx \varepsilon^{1/3}\lambda_0^{-2/3} \sim 10^5\ \mathrm{s}^{-1}$, as estimated from Eqs. (17) and (18), see Table 3. One sees that the obtained values of A_7 are in the range between ca. 1 and 10, and rapidly increase with the viscosity ratio, η_D/η_{EM}, which could be expected for drops with viscosity ratio higher than unity [49–51]. Note that these

Table 3
Properties of the emulsions studied in Section 6.2

η_D (mPa s)	Φ	d_{32} (μm)	d_{V95} (μm)	τ_0 (Pa)	c_η (Pa s^m)	m	$\varepsilon \times 10^{-5}$ (J/kg s)	λ_0 (μm)	$\dot{\gamma} \times 10^{-5}$ (s^{-1})
95	0.01	9.6	17.5	0	0.94×10^{-3}	1	2.7	1.3	5.4
95	0.2	8.2	18.8	0	1.5×10^{-3}	1	2.7	1.8	4.4
95	0.7	3.4	3.9	9	1.633	0.6167	3.7	10.8	1.5
95	0.8	2.4	2.6	29	12.46	0.4483	1.9	15.8	0.9
1024	0.7	3.4	7.2	<5	1.824	0.6505	4.4	16.0	1.2
1024	0.8	4.6	5.4	25	6.222	0.5777	2.1	31.9	0.6
10,000	0.8	10.7	30.5	<10	5.581	0.5768	1.7	31.3	0.6

Note. η_D is viscosity of the oil phase, Φ is oil volume fraction, d_{32} is mean volume-surface diameter, d_{V95} is maximum drop diameter by volume, τ_0 is emulsion yield stress, c_η is emulsion consistency, and m is power-law index in the stress vs shear rate dependence. The rate of energy dissipation, ε, is estimated from Eq. (16′); the size of the smallest eddies, λ_0, is estimated by Eq. (18); and the average shear rate in the smallest eddies, $\dot{\gamma}$, is estimated by Eq. (17).

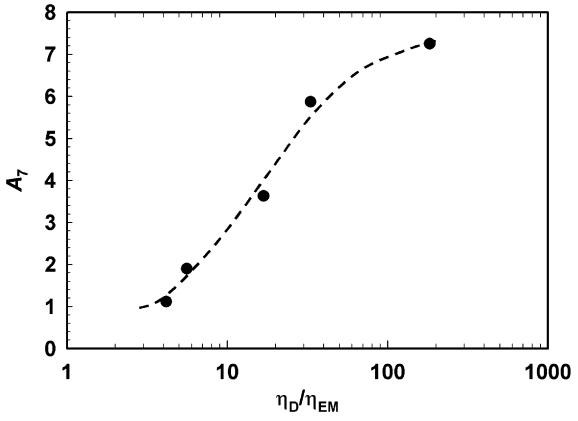

Fig. 13. Critical number, A_7, for breakup of silicone oil drops in viscous turbulent regime of emulsification, as a function of the viscosity ratio, η_D/η_{EM} (see Section 6.2 for explanations). The dashed curve is guide to the eye.

values of A_7 are similar in magnitude to $A_2 \approx 4$, which was determined in Section 6.1 for the viscous regime of emulsification with diluted emulsions prepared with viscous aqueous phase, $\eta_C > 3$ mPa s. This comparison is another indication that the smaller drops obtained in concentrated emulsions could be explained as a result of changing the regime of emulsification from inertial to viscous due to the increase of Φ.

The estimates performed above should be considered as a first approximation only, because the rate of energy dissipation was calculated from Eq. (16′), which might be inapplicable to such concentrated emulsions. However, the observed correct trends and the reasonable values of the estimated quantities indicate that Eqs. (17)–(19) can be used for approximate estimates in the case of concentrated emulsions.

6.3. Discussion—transition between inertial turbulent and viscous turbulent regimes of emulsification

The results described above and their interpretation show that the factors controlling the maximum drop size are different in the two regimes of turbulent emulsification. This difference is particularly important when emulsifying viscous oils, because much smaller droplets could be obtained in the viscous regime of emulsification, at equivalent other conditions. Therefore, it is important for the researchers and practitioners to be able to recognize which of these regimes is realized in their equipment and how one could switch between them.

For non-viscous oils, $\eta_D \approx \eta_C$, the respective analysis is straightforward, being based on the Kolmogorov–Hinze theory, Eqs. (1), (4), and (6). At known power dissipation energy, ε, one can estimate from these equations the size of the smallest eddies in the turbulent flow, λ_0, and the predicted drop diameters in the two regimes of emulsification, d_{KH} and d_{KV}. If these equations predict $\lambda_0 < d_{KH}$, then the emulsification occurs in the inertial regime of emulsification. In contrast, if the equations predict $d_{KV} < \lambda_0$, then the emulsification occurs in the viscous regime of emulsification. Finally, if the equations predict $d_{KH} \approx d_{KV} \approx \lambda_0$, the emulsification occurs in the transitional regime between the viscous and the inertial regimes. Note that Eqs. (4) and (6) are derived under the assumption $d_{KV} < \lambda_0 < d_{KH}$ and could be used to predict the actual drop size in these ranges only.

The results obtained in Sections 6.1 and 6.2 show that the above arguments are not applicable to emulsions of more viscous oils, because we see a significant effect of η_C on the maximum drop size, d_{V95}, even when the calculated values of d_D (Eq. (7)) are much larger than λ_0. For these oils, one could compare the maximum drop diameters, d_D and d_{KV}, as predicted by Eqs. (6) and (7). If the estimated sizes $d_{KV} > d_D > \lambda_0$, then the inertial forces are more efficient in breaking the drops and the emulsification is in the inertial regime. In the case, $d_{KV} < \lambda_0$, the emulsification occurs in the viscous regime, independently of the ratio of d_D and λ_0 (one can show theoretically that $d_{KV} < d_D$ in these systems). There is an intermediate case, in which the estimates show $d_D > d_{KV} > \lambda_0$, where it is not obvious which of the emulsification regimes is operative, because Eq. (6) for d_{KV} is not justified in this case. In our experiments, see Fig. 10, we interpreted the respective data as corresponding to the viscous regime of emulsification, because we detect a significant effect of η_C on the drop size (see the following paragraph). Note that for these theoretical estimates one should know the values of ε and A_2 (or A_7 for the non-Newtonian fluids), which makes this procedure not always feasible.

Alternatively, one could try to deduce the regime of emulsification for the viscous oils by investigating experimentally the effect of η_C on the drop size. If the drop size is not affected significantly by variations of the viscosity of the continuous phase in a relatively narrow range (e.g., up to 2–3 times), this is a good indication that the emulsification is in the inertial regime.

In contrast, if the drop diameter decreases with the increase of η_C and the experimental values of d_{V95} are smaller than λ_0, this is a good indication for a viscous regime of emulsification.

The analysis of Eqs. (1), (4), (6), and (7) shows that the most efficient factor for changing the regime of emulsification is the viscosity of the continuous phase, η_C, because it affects strongly λ_0 and d_{KV}, without affecting d_{KH} and d_D. In contrast, ε is not appropriate variable in this aspect, because it affects d_{KH}, d_D, and λ_0 in a similar way: $d_{KH}/\lambda_0 \propto \varepsilon^{-3/20}$ for non-viscous oils (negligible η_D in the drop breakup process) and $d_D/\lambda_0 \propto \varepsilon^0$ for viscous oils (negligible capillary pressure).

7. Conclusions

Systematic series of emulsification experiments is performed to quantify the effects of several factors on the mean drop size, d_{32}, the maximum drop size, d_{V95}, and the emulsion polydispersity after emulsification in turbulent flow. These factors include: oil viscosity, η_D, viscosity of the continuous phase, η_C, interfacial tension, σ, oil volume fraction, Φ, and rate of energy dissipation in the turbulent flow, ε. The results clarify that the emulsification could be performed in the two qualitatively different regimes predicted by the Kolmogorov's theory [12], inertial turbulent and viscous turbulent. The main observations and conclusions from the study could be summarized as follows:

Emulsification in inertial turbulent regime

- The mean and the maximum drop diameters increase with the increase of η_D and σ, and with the decrease of ε. In contrast, the mean drop size depends slightly on Φ and η_C in the inertial regime of emulsification.
- The emulsion polydispersity does not depend significantly on σ and ε, but increases strongly with the increase of oil viscosity, η_D.
- The inertial regime is inappropriate for emulsification of viscous oils with $\eta_D > 500$ mPa s, if drops of micrometer size have to be obtained.

Emulsification in viscous turbulent regime

- Transition from inertial to viscous turbulent regime of emulsification can be accomplished by a moderate increase of the viscosity of the aqueous phase ($\eta_C > 3$ mPa s in the studied systems) and/or by increase of the oil volume fraction, $\Phi > 0.6$.
- The viscous regime of emulsification is appropriate for emulsification of very viscous oils with η_D up to 10,000 mPa s. Typically, smaller drops are obtained in the viscous turbulent regime of emulsification (as compared to the inertial regime) at similar other conditions.
- The drop polydispersity for emulsions prepared with viscous silicone oils significantly decreases when the viscous regime is realized by increase of the oil volume fraction above 0.6. Apparently, the microstructure of the concentrated emulsions modifies the mode of drop breakup in the process of drop deformation, so that more uniform drops are formed.

Comparison of the experimental results with theoretical expressions

- The experimental data for the maximum drop size, d_{V95}, in the inertial regime of emulsification are reasonably well described by the Davies expression, Eq. (7), for all systems with $\eta_D < 500$ mPa s.
- The use of Eq. (7) to describe the mean drop size, d_{32}, has more limited application—to emulsions with similar polydispersities only (in our systems, for oils with $\eta_D <$ 100 mPa s).
- The numerical constants, which account for the contributions of the viscous dissipation inside the drops and for the surface deformation, are determined by interpreting our experimental data with Eq. (7) and by comparison with literature results. We found that Eq. (7) with $A_1 = A_3 = 0.86$ and $A_4 = 0.37$ predicts rather well d_{V95} for a wide range of oil viscosities, interfacial tensions, and hydrodynamic conditions during emulsification. These values are very close to those predicted theoretically by Davies [16], $A_3 \approx 1.0$ and $A_4 \approx 0.35$. The difference between the numerical values reported in the current study, and other values reported in literature, is explained with the different definitions of ε, used in the various studies.
- The maximum size of the droplets obtained in the viscous turbulent regime was successfully described by Eq. (6) (with $A_2 \approx 4$ for oil with viscosity 95 mPa s).
- The maximum size of the droplets obtained in concentrated emulsions was described by Eq. (19) with A_7 considered as a free parameter, depending on the viscosity ratio η_D/η_{EM}.

Acknowledgments

The authors of Ref. [40] are gratefully acknowledged for allowing us to use the data for dynamic interfacial tension prior to their publication. The valuable experimental help by D. Sidzhakova and the help in drop-size determination by M. Paraskova and E. Kostova (all from the Sofia University) are deeply appreciated. This study was supported by BASF Aktiengesellschaft, Ludwigshafen, Germany.

Appendix A. Notation

Capital Latin letters

A	dimensionless constants appearing in the equations for the drop diameter, d
A_1	Eq. (4)
A_2	Eq. (6)
A_3, A_4	Eq. (7)
A_5, A_6	Eq. (8)
A_7	Eq. (19)
A_σ, A_η	dimensionless constants accounting for the effects of the capillary pressure and of the viscous dissipation

inside the drop, respectively, in the process of drop deformation and breakage

C_1, C_2 dimensionless constants characterizing the turbulent flow in Kolmogorov's theory, Eq. (2)

D external diameter of the annular gap in the processing element

$F_V(d)$ cumulative distribution function by volume

$F_N(d)$ cumulative distribution function by number

H geometric width of the gap in the processing element, Eq. (15)

H_{hyd} characteristic hydrodynamic width of the gap, defined as $[4S/H_P]$

H_P wetted perimeter of the gap, defined as $[2\pi(D-H)]$

L total length of the gaps in the processing element, Eq. (15)

N_i number of drops with diameter d_i, measured by optical microscopy

P pressure

P driving pressure of the emulsification process

P_C drop capillary pressure

$\langle \Delta P_T(d) \rangle$ statistically averaged fluctuations in the dynamic turbulent pressure between two points separated at distance, d, from each other

Q flow rate of the emulsion through the homogenizer

Re Reynolds number of the fluid, defined as $\mathrm{Re} = \rho_C U_1 \times H_{hyd}/\eta_C$

S area of the gap cross-section, defined as $[\pi H(D-H)]$

U velocity

U_1 mean linear velocity of the fluid through the gap in the processing element, Eq. (15)

$\langle U^2 \rangle$ mean square fluctuations in the fluid velocity

$U_{\lambda 0}$ characteristic fluid velocity inside the smallest turbulent eddies

V volume

V_{DIS} effective volume, in which the main turbulent dissipation of energy occurs

V_{GAP} geometrical volume of one gap in the processing element

Small Latin letters

a constants of proportionality between the flow rate and the driving pressure during emulsification

a_{p1} for the pressure as a function of the flow rate for 1-slit processing element

a_{p2} for the pressure as a function of the flow rate for 2-slit processing element

a_{q1} for the flow rate as a function of the pressure for 1-slit processing element

a_{q2} for the flow rate as a function of the pressure for 2-slit processing element

c_η emulsion consistency, Eq. (13)

d drop diameter

d_C maximum diameter of stable Newtonian drops according to Eq. (8) (Calabrese et al. [18–21], inertial regime)

d_D maximum diameter of stable Newtonian drops according to Eq. (7) (Davies [16], inertial regime)

d_{KH} maximum diameter of stable drops at negligible viscosity of the drop phase according to Eq. (4) (Kolmogorov–Hinze [12,13], inertial regime)

d_{KI} group $(\varepsilon^{-2/5}\sigma^{3/5}\rho_C^{-3/5})$ with dimension of length, Eq. (4)

d_{KV} maximum diameter of the stable drops in the viscous regime of emulsification according to Eq. (6)

$d_{V,PL}$ maximum diameter of stable drops in a concentrated emulsion behaving as a power-law fluid, Eq. (19)

d_{32} experimentally measured mean volume-surface diameter

$\bar{d}_{10}$ geometric mean diameter by number in the log–normal distribution, Eq. (11)

d_{N50} experimentally measured mean diameter, 50% by number, Eq. (11)

$\bar{d}_V$ mean diameter by volume in the normal distribution, Eqs. (9) and (10)

d_{V50} experimentally measured mean diameter, 50% by volume, Eq. (10)

d_{V95} experimentally measured maximum drop diameter, 95% by volume

m power-law index characterizing the rheological properties of concentrated emulsion, Eq. (13)

q ratio (V_{DIS}/V_{GAP})

r^2 correlation coefficient

Capital Greek letters

Γ adsorption of the emulsifier on drop surface

Φ oil volume fraction

Small Greek letters

χ friction coefficient, Eq. (15)

ε rate of energy dissipation in the turbulent flow per unit mass of the fluid

$\bar{\varepsilon}_{gap}$ rate of energy dissipation, averaged over the volume of the gap in the processing element

$\dot{\gamma}$ shear rate

η dynamic viscosity

η_C viscosity of the continuous (aqueous) phase

η_D viscosity of the dispersed (oil) phase

η_{EM} effective viscosity of the emulsion at shear rate $\dot{\gamma} \sim 10^5\ \mathrm{s}^{-1}$

λ_0 size of the smallest turbulent eddies

ρ mass density

ρ_D mass density of the dispersed phase

ρ_C mass density of the continuous phase

σ equilibrium interfacial tension

$\sigma(t)$ dynamic interfacial tension

σ_{LN} dimensionless width of the log–normal distribution by number, Eq. (11)

σ_V dimensional width of the normal distribution by volume, Eq. (9)

τ stress

τ_0 yield stress of concentrated emulsion
τ_C viscous stress inside the turbulent eddies
τ_V viscous (shear rate-dependent) stress of the emulsion

Abbreviations

Betaine cocoamidopropyl betaine
Br, Brij, Brij 58 polyoxyethylene-20 hexadecyl ether
C16 hexadecane
ME membrane emulsification (Table S1)
Min27, Min150 mineral oils with viscosities 27 and 150 mPa s, respectively (Fig. 6)
Na caseinate, NaCas, NaC sodium caseinate
1S processing element with one slit (Fig. 8)
2S processing element with two slits (Fig. 8)
SBO soybean oil
SDP3S sodium dodecyl-polyoxyethylene-3 sulfate
SDS sodium dodecyl sulfate
Sil50, Sil100, Sil200, Sil500 silicone oils with different viscosities (Fig. 6)
WPC whey protein concentrate

Supplementary material

The online version of this article contains additional supplementary material.

Please visit DOI: 10.1016/j.jcis.2007.03.059.

References

[1] C.A. Coulaloglou, L.L. Tavlarides, Chem. Eng. Sci. 32 (1977) 1289.
[2] C. Tsouris, V.I. Kirou, L.L. Tavlarides, AIChE J. 40 (1994) 407.
[3] C. Tsouris, L.L. Tavlarides, AIChE J. 40 (1994) 395.
[4] M.J. Prince, H.W. Blanch, AIChE J. 36 (1990) 1485.
[5] M.M. Razzaque, A. Afacan, Sh. Liu, K. Nandakumar, J.H. Masliyah, R.S. Sanders, Int. J. Multiphase Flow 29 (2003) 1451.
[6] A.M. Kamp, A.K. Chesters, C. Colin, J. Fabre, Int. J. Multiphase Flow 27 (2001) 1363.
[7] N. Vankova, S. Tcholakova, N.D. Denkov, V. Vulchev, T. Danner, Emulsification in turbulent flow: 2. Breakage rate constants. Second paper of this series.
[8] S. Tcholakova, N. Vankova, N.D. Denkov, T. Danner, Emulsification in turbulent flow: 3. Daughter drop-size distribution, J. Colloid Interface Sci. (2007), doi:10.1016/j.jcis.2007.01.097, in press.
[9] M. Kostoglou, A.J. Karabelas, Chem. Eng. Sci. 53 (1998) 505.
[10] M. Kostoglou, A.J. Karabelas, Chem. Eng. Sci. 56 (2001) 4283.
[11] M. Kostoglou, A.J. Karabelas, Chem. Eng. Sci. 60 (2005) 6584.
[12] A.N. Kolmogorov, Compt. Rend. Acad. Sci. URSS 66 (1949) 825.
[13] J.O. Hinze, AIChE J. 1 (1955) 289.
[14] F.B. Sprow, Chem. Eng. Sci. 22 (1967) 435.
[15] H.T. Chen, S. Middleman, AIChE J. 13 (1967) 989.
[16] J.T. Davies, Chem. Eng. Sci. 40 (1985) 839.
[17] J.S. Lagisetty, P.K. Das, R. Kumar, K.S. Gandhi, Chem. Eng. Sci. 41 (1986) 65.
[18] R.V. Calabrese, T.P.K. Chang, P.T. Dang, AIChE J. 32 (1986) 657.
[19] C.Y. Wang, R.V. Calabrese, AIChE J. 32 (1986) 667.
[20] R.V. Calabrese, C.Y. Wang, N.P. Bryner, AIChE J. 32 (1986) 677.
[21] P.D. Berkman, R.V. Calabrese, AIChE J. 34 (1988) 602.
[22] P. Walstra, in: Encyclopedia of Emulsion Technology, Dekker, New York, 1983, Chapter 2.
[23] P. Walstra, in: J. Lyklema (Ed.), Fundamentals of Interface and Colloid Science: Soft Colloids, Academic Press, 2005, Chapter 8.
[24] J. Baldyga, W. Podgorska, Canadian J. Chem. Eng. 76 (1998) 456.
[25] S. Tcholakova, N.D. Denkov, D. Sidzhakova, I.B. Ivanov, B. Campbell, Langmuir 19 (2003) 5640.
[26] S. Tcholakova, N.D. Denkov, T. Danner, Langmuir 20 (2004) 7444.
[27] H. Steiner, R. Teppner, G. Brenn, N. Vankova, S. Tcholakova, N.D. Denkov, Chem. Eng. Sci. 61 (2006) 5841.
[28] V. Cristini, J. Blawzdziewicz, M. Loewenberg, L.R. Collins, J. Fluid Mech. 492 (2003) 231.
[29] C.A. Sleicher, AIChE J. 8 (1962) 471.
[30] J.F. Walter, H.W. Blanch, Chem. Eng. J. 32 (1986) B7.
[31] S.M. Bhavaraju, T.W.F. Russel, H.W. Blanch, AIChE J. 24 (1978) 454.
[32] G.K. Batchelor, An Introduction to Fluid Dynamics, Cambridge, 1967.
[33] L. Svarovsky, in: Solid–Liquid Separation, Butterworths, London, 1981, Chapter 2.
[34] A.G. Gaonkar, R.P. Borwankar, Colloids Surf. 59 (1991) 331.
[35] O. Sather, in: J. Sjöblom (Ed.), Encyclopedic Handbook of Emulsion Technology, Dekker, New York, 2001, Chapter 15.
[36] P.S. Denkova, S. Tcholakova, N.D. Denkov, K.D. Danov, B. Campbell, C. Shawl, D. Kim, Langmuir 20 (2004) 11402.
[37] H.M. Princen, in: J. Sjöblom (Ed.), Encyclopedia of Emulsion Technology, Dekker, New York, 2001, Chapter 11, p. 243.
[38] T.G. Mason, Rheology of monodisperse emulsions, Ph.D. thesis, Department of Physics, Princeton University, 1995.
[39] N.D. Denkov, V. Subraminian, D. Gurovich, A. Lips, Colloids Surf. A 263 (2005) 129.
[40] D. Dimitrova, V. Vulchev, et al., in preparation.
[41] T. Horozov, L. Arnaudov, J. Colloid Interface Sci. 219 (1999) 99.
[42] T. Horozov, L. Arnaudov, J. Colloid Interface Sci. 222 (2000) 146.
[43] L.D. Landau, E.M. Lifshitz, Theoretical Physics, Hydrodynamics, vol. VI, Nauka, Moscow, 1988 [in Russian].
[44] L.A. Cutter, AIChE J. 12 (1966) 34.
[45] X. Gutierrez, F. Silva, M. Chirinos, J. Leiva, H. Rivas, J. Dispersion Sci. Technol. 23 (2002) 405.
[46] K.M.B. Jansen, W.G.M. Agterof, J. Mellema, J. Rheol. 45 (2001) 227.
[47] C.F. Welch, G.D. Rose, D. Malotky, S.T. Eckersley, Langmuir 22 (2006) 1544.
[48] A.M. Kraynik, Annu. Rev. Fluid Mech. 20 (1988) 325.
[49] H.P. Grace, Chem. Eng. Commun. 14 (1982) 225.
[50] J.M. Rallison, Annu. Rev. Fluid Mech. 16 (1984) 45.
[51] H. Stone, Annu. Rev. Fluid Mech. 26 (1994) 65.